Materials Today Bio 28 (2024) 101196

Contents lists available at ScienceDirect

Materials Today Bio

journal homepage: www.journals.elsevier.com/materials-today-bio

Hybrid construction of tissue-engineered nerve graft using skin derived precursors induced neurons and Schwann cells to enhance peripheral neuroregeneration

Qi Guo [a,1], Hui Zhu [b,1], Xi Xu [c,d,1], Tianyi Huang [d], Yulin Pan [d], Xiaosong Gu [b,**], Shusen Cui [a,***], Chengbin Xue [b,*]

[a] Department of Hand and Foot Surgery, China-Japan Union Hospital of Jilin University, Key Laboratory of Peripheral Nerve Injury and Regeneration of Jilin Province, The Third Bethune Hospital of Jilin University, Changchun, JL, 130033, PR China
[b] Research Center of Clinical Medicine, Affiliated Hospital of Nantong University, Key Laboratory of Neuroregeneration of Jiangsu and Ministry of Education, Co-Innovation Center of Neuroregeneration, NMPA Key Laboratory for Research and Evaluation of Tissue Engineering Technology Products, Nantong University, Nantong, JS, 226001, PR China
[c] Department of Rehabilitation Medicine, Affiliated Hospital of Nantong University, Nantong, JS, 226001, PR China
[d] Medical School of Nantong University, Nantong, JS, 226001, PR China

ARTICLE INFO

Keywords:
Skin derived precursor
Neuroregeneration
Tissue engineered nerve graft
Peripheral nerve injury
Schwann cell
Neuron

ABSTRACT

Peripheral nerve injury is a major challenge in clinical treatment due to the limited intrinsic capacity for nerve regeneration. Tissue engineering approaches offer promising solutions by providing biomimetic scaffolds and cell sources to promote nerve regeneration. In the present work, we investigated the potential role of skin-derived progenitors (SKPs), which are induced into neurons and Schwann cells (SCs), and their extracellular matrix in tissue-engineered nerve grafts (TENGs) to enhance peripheral neuroregeneration. SKPs were induced to differentiate into neurons and SCs *in vitro* and incorporated into nerve grafts composed of a biocompatible scaffold including chitosan neural conduit and silk fibroin filaments. *In vivo* experiments using a rat model of peripheral nerve injury showed that TENGs significantly enhanced nerve regeneration compared to the scaffold control group, catching up with the autograft group. Histological analysis showed improved axonal regrowth, myelination and functional recovery in animals treated with these TENGs. In addition, immunohistochemical staining confirmed the presence of induced neurons and SCs within the regenerated nerve tissue. Our results suggest that SKP-induced neurons and SCs in tissue-engineered nerve grafts have great potential for promoting peripheral nerve regeneration and represent a promising approach for clinical translation in the treatment of peripheral nerve injury. Further optimization and characterization of these engineered constructs is warranted to improve their clinical applicability and efficacy.

1. Introduction

Peripheral nerve injuries remain a significant clinical challenge due to their limited intrinsic regenerative capacity [1]. Despite advancements in surgical techniques and rehabilitation strategies, many patients experience persistent sensory and motor deficits following nerve trauma [2]. The diverse approaches and emerging technologies being explored to enhance nerve regeneration. By leveraging cell-based therapies, biomaterials, growth factors, and other innovative strategies, researchers are striving to develop more effective treatments for peripheral nerve injuries [3]. These advancements not only contribute to our understanding of nerve regeneration mechanisms but also offer promising avenues for translating these findings into clinical practice [4]. Tissue engineering approaches have emerged as promising solutions by providing biomimetic scaffolds and cell sources to promote peripheral nerve regeneration [5].

* Corresponding author.
** Corresponding author.
*** Corresponding author.
E-mail addresses: nervegu@ntu.edu.cn (X. Gu), cuiss@jlu.edu.cn (S. Cui), xue_chengbin@hotmail.com (C. Xue).
[1] Contributed equally to this work.

https://doi.org/10.1016/j.mtbio.2024.101196
Received 16 June 2024; Received in revised form 7 August 2024; Accepted 8 August 2024
Available online 9 August 2024

Schwann cells (SCs) are the primary glial cells responsible for regeneration and repair in the peripheral nervous system (PNS). However, the availability of sufficient donor material for SC-based therapies remains a major hurdle [6]. Recent advances in stem cell technologies have opened up new possibilities for generating engineered therapeutic SCs from a variety of accessible cell sources [7]. The importance of cell-based therapies and biomaterials in nerve regeneration has been further emphasized by current studies [8–10]. Skin-derived precursors (SKPs) are a population of multipotent stem cells located in the dermal layer of the skin. These cells exhibit remarkable plasticity and are able to differentiate into a variety of cell lineages, including neurons and SCs [6]. SKPs have attracted attention as a potential source of cells for tissue engineering applications due to their accessibility and their regenerative potential [11]. These advancements highlight the ongoing efforts to refine tissue engineering strategies for peripheral nerve repair and offer insights into potential avenues for future research.

One promising approach involves the use of stem cells and progenitor cells, which have the potential to differentiate into various cell types, including neurons and glial cells [12,13]. Among the various stem cell sources, SKPs have emerged as an attractive option for several reasons. SKPs can be easily and non-invasively harvested from skin biopsies, offering a readily accessible and abundant source of progenitor cells. SKPs can further develop into functional neurons and glial cells, including SCs. Using a patient's own SKPs for therapy reduces the risk of immune rejection and eliminates the need for immunosuppressive drugs [14,15]. SKPs secrete a variety of growth factors and cytokines that can promote a regenerative microenvironment, supporting the survival and growth of existing nerve cells and the integration of newly generated neurons. SKPs have been shown to modulate the immune response, which is crucial for creating a conducive environment for nerve repair following injury [6].

SKP-derived neurons may exhibit different patterns of electrical activity and synaptic connectivity compared to neurons derived from other sources, such as neural stem cells. SKPs have unique immunomodulatory effects that can influence the inflammatory response, which is a critical factor in the success of nerve regeneration [15]. The ability of SKP-derived cells to integrate into the host tissue and form functional connections with existing neurons may differ from that of SCs or other cell types. The use of SKPs may be subject to different regulatory requirements and manufacturing processes compared to more established cell sources like SCs, which have a longer history of clinical use. The use of SKPs avoids some of the ethical concerns associated with the use of embryonic stem cells or induced pluripotent stem cells. The use of SKPs in nerve regeneration offers a promising alternative to traditional cell sources due to their accessibility, differentiation potential, and unique properties. However, a comprehensive understanding of their behavior, integration, and functional outcomes is essential to optimize their therapeutic potential. Comparative studies with other cell sources, such as SCs, are crucial to elucidate the distinct advantages and limitations of SKPs in the context of nerve repair.

Our previous work identified cell types in the sciatic nerve of adult rats [16]. The neurons were distributed along the sciatic nerves from distal to proximal, which were present in both the crush model and normal rats. Moreover, extracellular matrix (ECM) components enhanced SCs migration and promoted axonal regrowth, leading to accelerated nerve repair. These findings underscore the importance of ECM-based biomaterials in providing cues for nerve regeneration [6,17,18]. Therefore, we would like to construct tissue-engineered neural grafts (TENGs) using SKPs induced differentiated neurons and SCs *in vitro* joint with their ECM, silk fibroin fiber and chitosan neural conduits to mimic the real sciatic nerve cellular components and microenvironment.

In the present work (Fig. 1 top), we investigate the potential of utilizing SKPs induced neurons and SCs in TENGs to enhance peripheral neuroregeneration. SKPs, a type of multipotent stem cell found in the skin, offer a readily accessible and abundant cell source for tissue engineering applications. By inducing SKPs into neurons and SCs *in vitro*, we aim to harness their regenerative potential for peripheral nerve repair. The TENGs are fabricated using a combination of induced SKPs and biocompatible scaffold materials, including chitosan neural conduit and silk fibroin filaments, to mimic the natural microenvironment of nerves. Chitosan, a biocompatible and biodegradable polymer, served as the neural conduit. This scaffold provides physical support and guidance for axonal growth. Silk fibroin, derived from silkworm cocoons, was used to reinforce the scaffold. Silk fibroin possesses excellent mechanical properties and promotes cell attachment and proliferation. *In vivo* experiments are conducted using a rat model of peripheral nerve injury to evaluate the efficacy of these engineered constructs in promoting nerve regeneration. The present work provides valuable insights into the potential of SKPs in peripheral nerve regeneration and lays the groundwork for future research aimed at overcoming the challenges in translating SKP research to clinical applications. The development of effective strategies for enhancing the survival, differentiation, and integration of SKPs could pave the way for novel therapeutic approaches in peripheral nerve repair.

2. Results

2.1. Isolation of SKPs and induced differentiation of SKP-neurons and SKP-SCs

Following the culture method of SKPs in nature protocols [19], SKPs were seeded into the medium at a density of 10^5/ml. Initially, SKPs were small, round, and had a high nucleus-to-cytoplasm ratio. SKPs grew in spherical suspension (Fig. 1a). They may express markers typical of stem cells, such as fibronectin (Fig. 1b), nestin (Fig. 1c), sca1 (Fig. 1d), versican (Fig. 1e) and vimentin (Fig. 1f). During the early neuronal differentiation, SKPs start to elongate and develop neurites (early signs of axons and dendrites). After about 5 days of differentiation culture, a distinct colony of cells was seen to emerge in the form of nests (Fig. 1g). The cells exhibit a more complex morphology with extensions that begin to form synapses. After continuing to culture with induced differentiation medium for one-week, neuronal morphology cells were seen to appear (Fig. 1h). For mature neuronal phenotype, neurons derived from SKPs have a distinct morphology with a cell body (soma), dendrites, and a single axon. The presence of dendritic spines and axonal varicosities can be observed, indicative of synaptic connections. Immunocytochemical staining showed positive expression of markers such as NF-200 and Beta III-tubulin (Fig. 1j-j4, ki-k4). NF-200 is a component of neurofilaments found in mature neurons. Its expression indicates the neuronal maturity and axonal development. βIII-tubulin is a tubulin isotype that is a component of microtubules and is expressed in post-mitotic neurons. It is often used as a marker for neuronal differentiation. SKP monocytes induced to differentiate under SKP-SCs differentiation medium showed typical SKP-SCs cell colonies with bipolar or tripolar cell morphology at around 2w, which were carefully digested with a small filter paper sheet and then expanded and cultured. For SCs differentiation, SKPs differentiating into SCs will lose their neuronal morphology and adopt a flat, spindle-shaped appearance. These cells will align and wrap around axons in a manner characteristic of

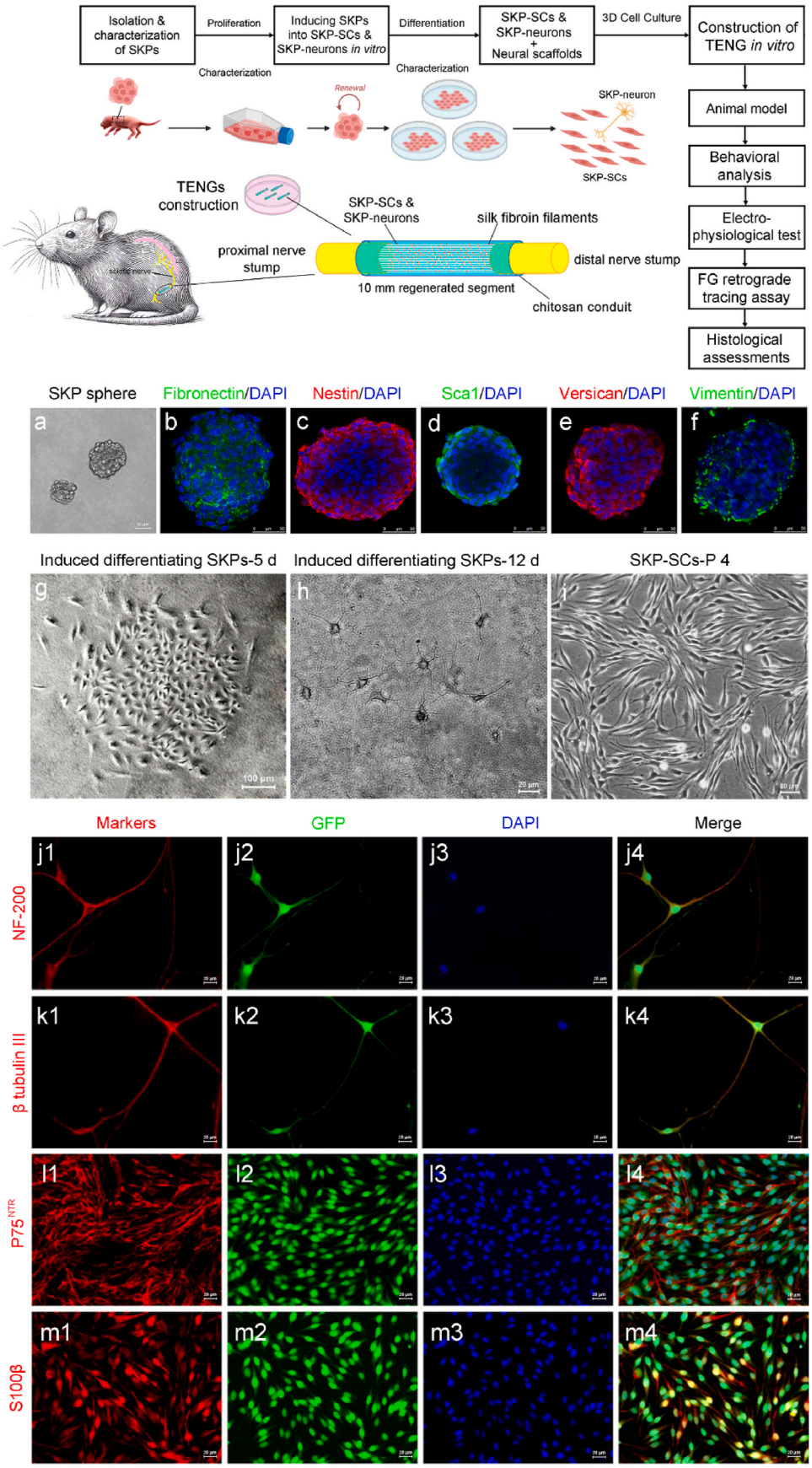

(caption on next page)

Fig. 1. Schematic illustration of the present work and isolation, differentiation and characterization of SKPs, SKP-neurons and SKP-SCs. Schematic illustration (top) of a skin-derived precursor (SKP)-induced Schwann cell and SKP-induced neurons-mediated tissue-engineered nerve graft (TENG) for rat sciatic nerve repair. The consisting of chitosan nerve conduit, inserted silk fibroin fibers, SKP-neurons, SKP-SCs and their extracellular matrix can promote sciatic nerve regeneration and functional restoration nearly to the levels achieved by autologous nerve grafts according to comprehensive analysis including behavioral, electrophysiological, FG retrograde tracing, and histological evidence. (a) SKP spheres were generated from juvenile SKPs post 14 days of culture. (b–f) Characterizations by the immunostainings of fibronectin (green), nestin (red), sca-1(green), versican (red), and vimentin(green) for SKPs. (g) SKP spheres were induced to differentiate into SKP-neurons (h) and SKP-SCs (i) *in vitro*. (c) The characterization of SKP-neurons and SKP-SCs by immunostainings of NF200 (j1-j4), β tubulin III (k1-k4) for SKP-neurons and p75 ^{NTR} (l1-l4), S100β (m1-m4) for SKP-SCs. (red) neurons and SCs markers, (green) GFP, (blue) DAPI. Scale bar: 50 μm for a-f, 100 μm for g, and 20 μm for h-m.

myelinating SCs (Fig. 1i). Immunocytochemical staining showed positive expression of SCs markers such as P75 and S100β (Fig. 1l1-l4, m1-m4). S100β is a calcium-binding protein typically expressed in Schwann cells and other cells of the nervous system. Its presence is indicative of the glial phenotype and is associated with processes like myelination and nerve repair. P75^{NTR} is a receptor found on many cell types of the nervous system, including neurons and glial cells. It is involved in neuronal survival, differentiation, and myelin formation, and can be a marker for neural crest-derived cells. These data demonstrated the successful isolation of SKPs and the inducing differentiation into SKP-SCs and SKP-neurons.

2.2. Construction and characterization of constructed SKP-TENGs

SKP-Neurons and SKP-SCs were collected by digestion and centrifugation and mixed (1:20) and seeded into silk fibroin filaments (Fig. 2a, 2a′) and chitosan neural conduit (Fig. 2c, c′, 2e, 2e′, 2g, 2g′). The cells were adhered to the surface of silk fibroin filaments and in the chitosan conduits. After adhering to the walls, they were cultivated for 14 days in a cell co-culture stimulated culture with a medium containing ascorbic acid to stimulate the secretion of ECM. Scanning electron microscopy showed that silk fibroin filaments in normal conditions were cylindrical with a uniform circumference and a smooth surface (Fig. 2b, b′). Chitosan conduits had a loose and porous outer wall (Fig. 2d, d′), a relatively dense inner wall, and many inter-tubular gaps (Fig. 2f, f′). After SKP-Neurons and SKP-SCs were seeded to the chitosan neural conduit and silk fibroin filaments, the cells were adhered to the walls of the conduits and the filamentous protein filaments, and in the case of the mixed cells, they were adhered to the walls of chitosan neural conduit and silk fibroin filaments. Protein filaments, which showed a tendency to be distributed along the longitudinal axis of the filaments (Fig. 2a, a′). Inside the tube wall, the cell morphology showed two different types of cells: asterisk-like long axonemal cells and bipolar cells, with small spherical granules outside the cells (Fig. 2e, e'). Immunocytochemical staining showed that the cells were tightly adhered to the scaffold material. Some cells showed positive expression of S100β and P75^{NTR} (Fig. 2i and j) and some cells showed positive expression of NF-200 and βIII-tubulin (Fig. 2k, l). The extracellular matrix components of collagen I, collagen IV, and laminin showed positive expression (Fig. 2m-o).

2.3. Behavioral test and neuro-electrophysiological analysis

To investigate whether SKP-Neurons and SKP-SCs mediate TENGs could enhance sciatic nerve functional recovery 12 w post nerve bridging surgery, behavioral test at 4-, 8- or 12-weeks, and neuro-electrophysiological analysis at 12 w were carried out separately. The CatWalk™ gait analysis system was utilized to calculate the sciatic function index (SFI) to monitor sciatic nerve functional recovery. At 4-, 8- or 12-weeks post-surgery, SFI values of both TENG and autograft groups were significantly better than that of the scaffold group (Fig. 3a–c). As expected, SFI values of the nongrafted group were consistently least than all other groups at all time points post-surgery.

To further evaluate to functional recovery, the amplitude of compound muscle action potential (CMAP) recordings and the nerve motor conduction velocity (MCV) calculations were performed in animals among different groups at 12 weeks post-surgery (Fig. 3d–j). CMAP amplitude of both nerve stumps and MCV in both TENG and autograft groups were superior than those in the scaffold group, and no significant difference was observed in CMAP between the TENG and autograft groups (Fig. 3h and i). All the grafted group did not fully return to normal levels (Fig. 3j).

2.4. Tracing of seed cells in vivo and SKP-TENGs promote axonal regrowth

To investigate the role of SKP-SCs during neuroregeneration, the GFP-SKP-Neurons and GFP-SKP-SCs were cultured on a silk fibroin filament-chitosan conduit. At three weeks post-implantation of the TENGs, amount of GFP-SKP-SCs were observed at the implantation site, suggesting that SKP-SCs contained in the TENG could survive at least three weeks after implantation (Fig. 4a–d and 4a′-4d′). The burst axon regeneration happened two weeks post-surgery (Fig. 4e).

To examine whether SKP-Neurons and SKP-SCs TENGs can help axons regrow, TENG, scaffold, and autograft were applied to bridge the 10-mm sciatic nerve in rats, respectively. The cryo-longitudinal-section and immunofluorescence labeling (NF200) were carried out in all grafted groups at 1 w and 2 w post nerve bridging surgery (Fig. 4f–h and 4j-4l). Axon regeneration distance in both TENG and autograft groups were superior than those in the scaffold group, and no significant difference was observed between the TENG and autograft groups (Fig. 4i, m).

To obtain the histological evaluation of regenerated nerves harvested at 12 weeks post-surgery, the transverse sections of the distal nerve stump stained by NF200 (Fig. 5a1-5e1) and S100β antibodies (Fig. 5a2-5e2) indicated that massive bundles of myelinated nerve fibers dispersed in clusters in both the TENG and autograft groups, despite appearing disorganized than normal group. Contrarily, inferior axonal regeneration was investigated in scaffold group. And none regenerated nerve fibers were observed in the nongrafted group (Fig. 5a3-5e3). The density of regenerated nerve fibers was significantly higher in both the TENG and autograft groups than in the scaffold group. However, all the grafted groups did not catch up the normal control. All these data indicate that SKP-Neurons and SKP-SCs based TENGs can promote axonal regeneration.

2.5. Functional evaluation of SKP-TENGs via nerve tracing

Fluoro-Gold™ (FG) is a very effective and commonly used neurotransmitter among retrograde tracers [20]. One weeks after FG was injected into the distal part of the nerve graft (the same location on the normal side as on the operated side of the injection), neurons in the spinal cord (Fig. 6a, c, e, g and Fig. 6a′, c′, e′, g′) and dorsal root ganglia (Fig. 6b, d, f, h and Fig. 6b′, d′, f′, h′) of the corresponding segment on the injected side were labeled and fluoresced with gold color under UV

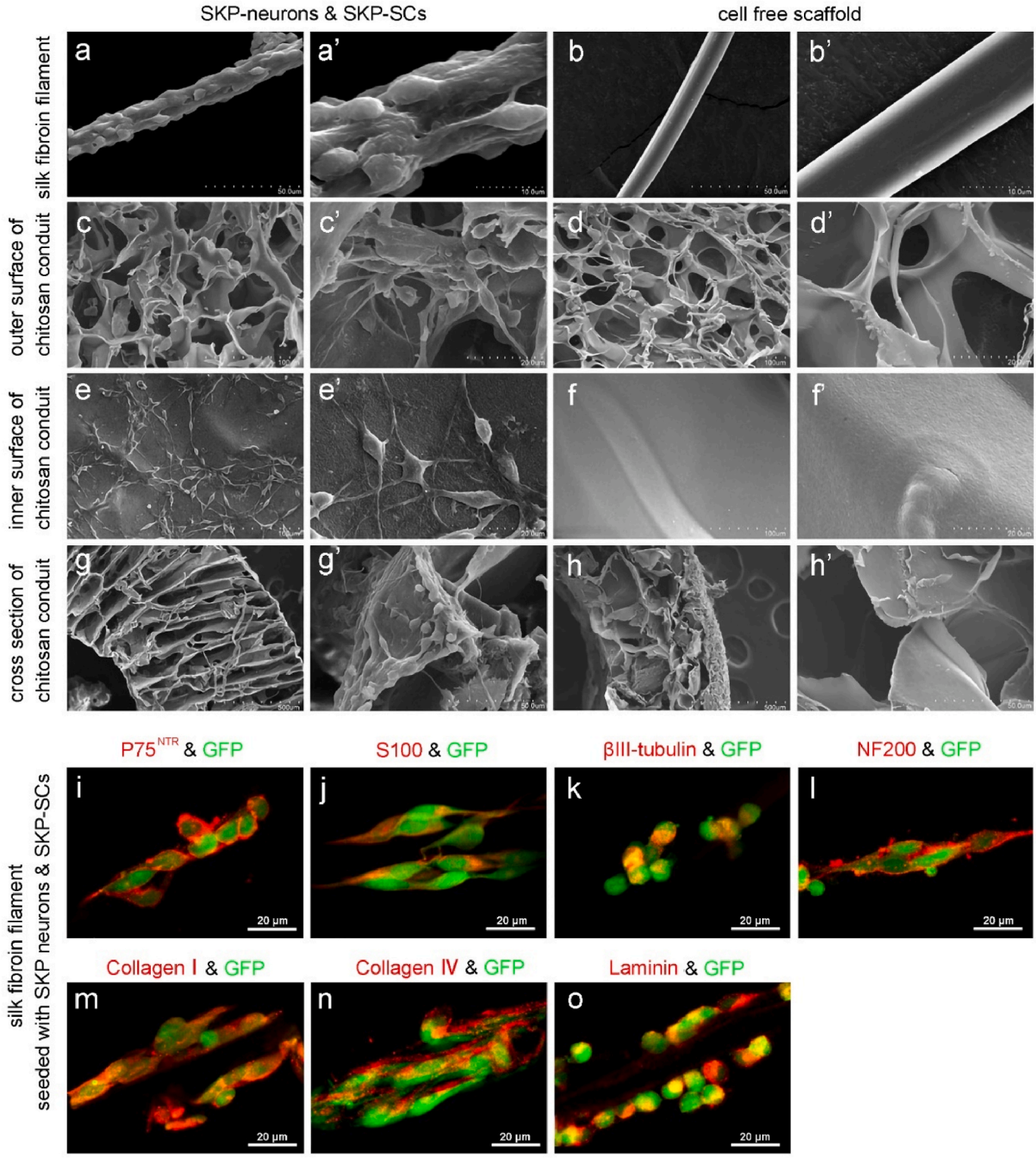

Fig. 2. Construction of TENGs *in vitro*. (a–h) SEM images and (i–o) immunofluorescence images showed the micromorphology of GFP-SKP-neurons and GFP-SKP-SCs cultured on silk fibroin filaments and chitosan conduit 14 days post construction of TENGs. SCs markers (p75 ^{NTR} and S100 β), neurons markers (β tubulin III and NF200) and ECM molecules (collagen I, collagen IV, and laminin) were confirmed by immunostainings on the silk fibroin filaments.

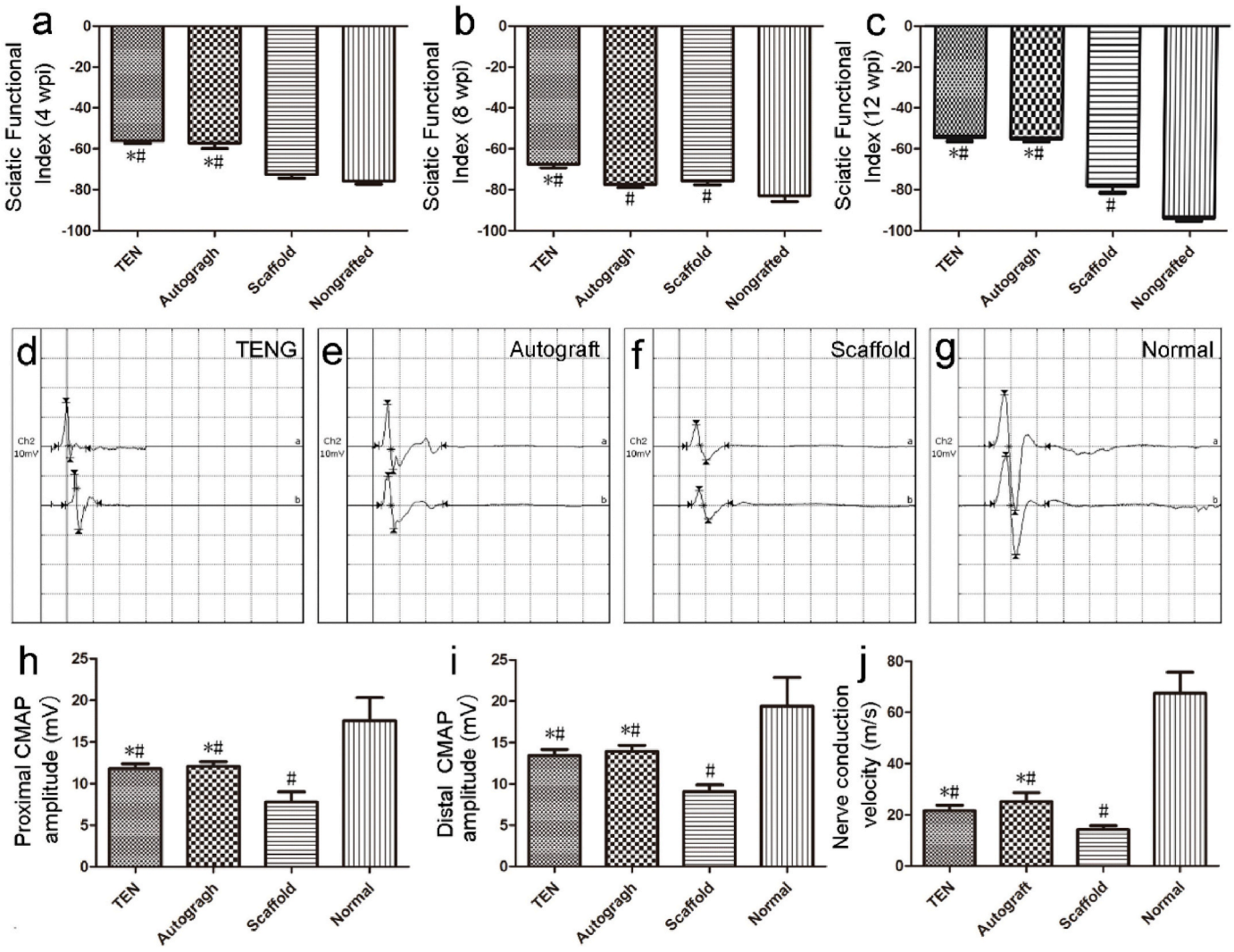

Fig. 3. The locomotor function and electrophysiological evaluation of TENGs on sciatic nerve functional recovery. (a–c) Histogram comparing the SFI values among four groups at 4 w, 8 w, and 12 w post-surgery. $^{*}p < 0.05$ versus scaffold group and $^{\#}p < 0.05$ versus nongrafted group. (d–g) Representative CMAP recordings at 12 weeks post-surgery, were obtained from the injured side of animals in TENG, autograft, scaffold groups and on the contralateral uninjured side (normal) of animals, respectively. (h–j) Histograms showing the proximal and distal CMAP amplitude detected on the injured side of animals, and the motor nerve conduction velocity and in the TENG, autograft, scaffold groups and on the contralateral uninjured side (normal), respectively. $^{*}p < 0.05$ versus scaffold group and $^{\#}p < 0.05$ versus normal group.

excitation. In the spinal cord, the fluorescent gold-positive cells were distributed in clusters, and the fluorescent gold-positive neurons in the dorsal root ganglia were arranged axially and tended to cluster on one side. The cells in the spinal cord were counted with clear cytosol outlines and fluorescent gold-positive cells, and the total number of fluorescent gold-positive cells in all longitudinal sections of each spinal cord was calculated separately. No obvious difference was observed between the TENG and autograft groups either in the total number of FG-labeled motor neurons (Fig. 6i) or the percentage of FG-labeled sensory neurons (Fig. 6j). Notably, significantly more neurons in the TENG and autograft groups were labeled with FG than those in the scaffold group, suggesting a superior reconstruction of neural pathway and axonal transportation in the former groups.

2.6. Ultrastructural assessment of sciatic nerve regeneration via SKP-TENGs

(Fig. 7a–e) Transmission Electron Microscopy (TEM) further demonstrated that after grafting with TENGs or autologous nerve grafts, numerous unmyelinated and myelinated nerve fibers were dispersed in clusters, and the myelinated axon was surrounded by a clear, thick, and electron-dense myelin sheath, which was thinner than that on the contralateral uninjured side (Fig. 7e, e′). The lamellae structure of regenerated myelin sheaths provided further evidence for this observation (Fig. 7a'-7e′). The disoriented distribution of cells in degenerated fascicules and obvious hyperplasia of connective tissues without regenerated nerve fibers. No regenerated nerve fibers but obvious hyperplasia of

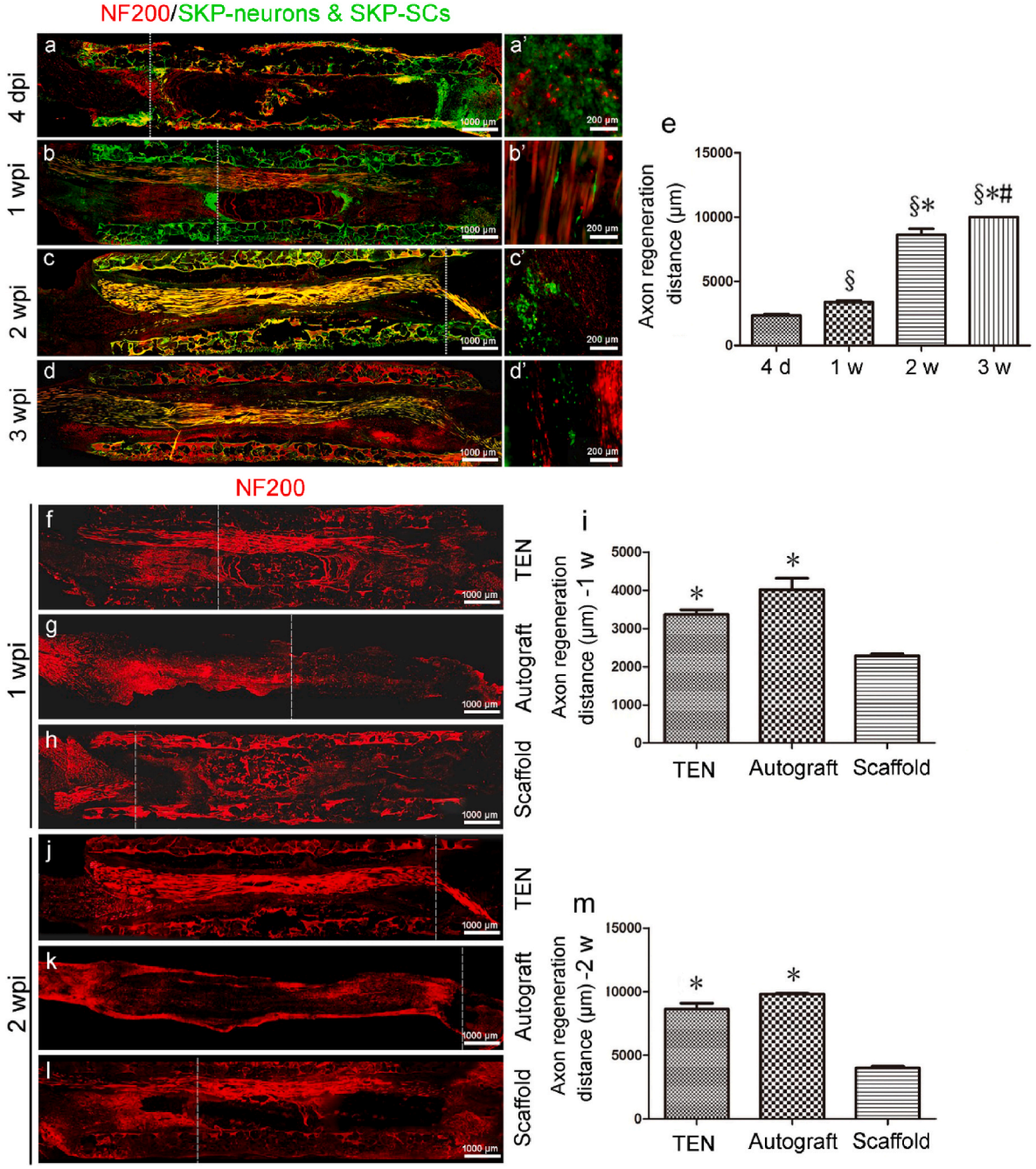

Fig. 4. Evaluation of axonal regeneration on TENGs after nerve bridging surgery. (a–d) The immunofluorescence images of the longitudinal sections of TENGs at 4 dpi, 1, 2, 3 weeks post-surgery. (a'-d') are the local magnified fields of (a–d). The dashed lines indicate regenerating axon terminals. (e) Histogram of the axon regeneration distances at the proximal stumps of TENGs are calculated (n = 8). The SKP-neurons and SKP-SCs are illustrated (GFP, green). The axons are NF200 positive, red. Scale bar, 1000 μm and 200 μm respectively. $^{§}p < 0.05$ versus 4 d, $^{*}p < 0.05$ versus 1 w, and $^{\#}p < 0.05$ versus 2 w. (f–l) The immunofluorescence images of the longitudinal sections of TENG, autograft, and scaffold groups at 1, 2 weeks post-surgery. The dashed lines indicate regenerating axon terminals. The NF200 positive axons are illustrated in red. (i, m) Histograms of the axon regeneration distances of TENG, autograft, and scaffold groups are calculated at 1, 2 weeks post-surgery (n = 8). $^{*}p < 0.05$ versus scaffold group.

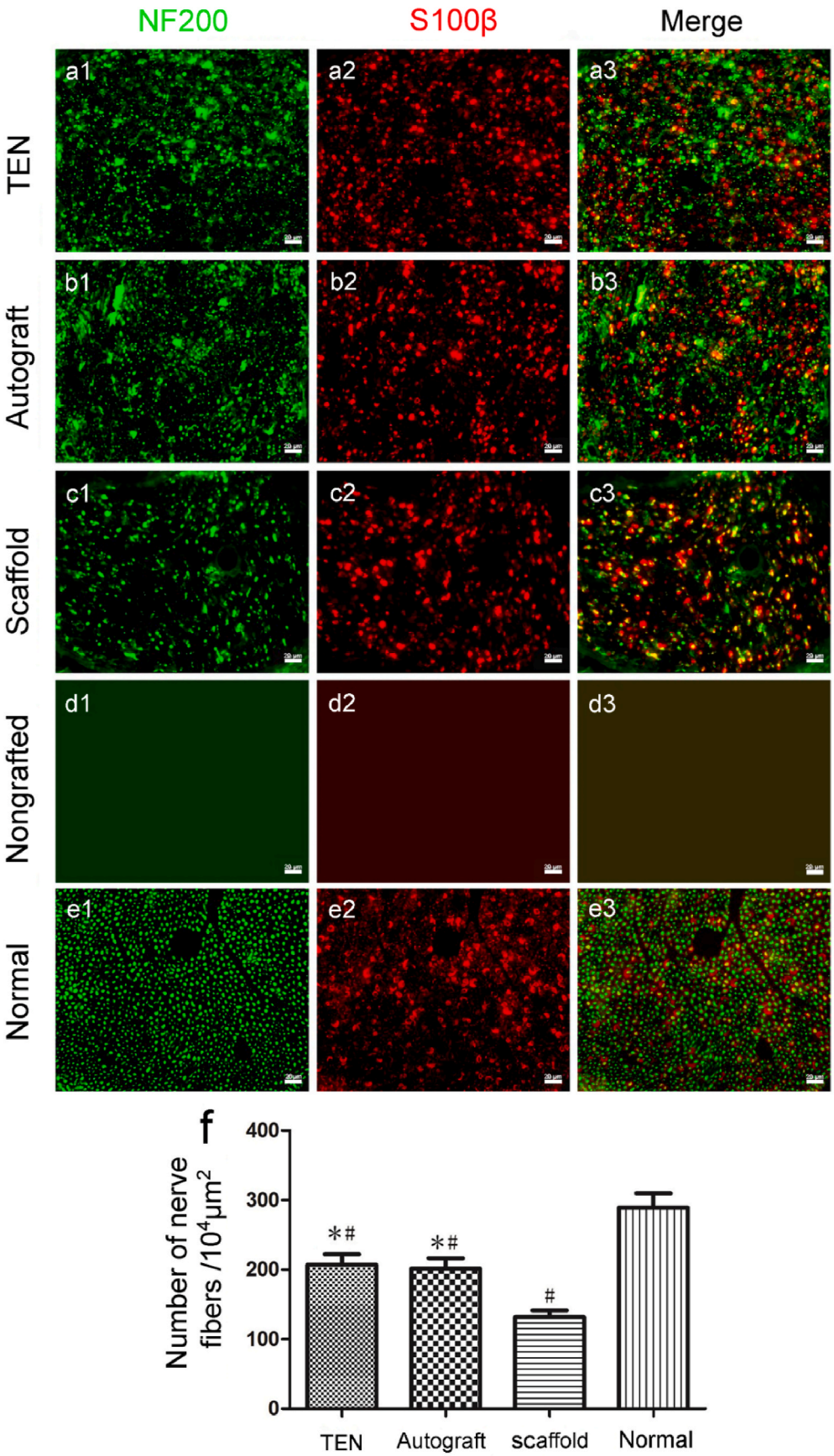

(caption on next page)

Fig. 5. Analysis of regenerated axon density post-surgery. (a–e) The immunofluorescence images of the cross sections of regenerated nerve distal portion to TENG, autograft, scaffold groups and the contralateral uninjured side (normal). (a1-e1) The NF200 positive axons are illustrated in green. (a2-e2) The S100β Schwann cells or myelin structure are illustrated in red. Scale bar, 500 μm and 100 μm respectively. (f) Histogram of the regenerated axon density were shown and analyzed (n = 8). $^{*}p < 0.05$ versus scaffold group and $^{\#}p < 0.05$ versus normal group.

connective tissues and disoriented arrangement of fusiform cells in degenerated fascicules were visible in non-grafted group (Fig. 7d and d′). Morphometric analysis revealed that parameters, such as the thickness of myelin sheath (Fig. 7f), diameter of myelinated nerve fibers (Fig. 7g), and number of myelin lamellae (Fig. 7h), parameters measured on the injured side were significantly lower than those on the contralateral uninjured side, which also indicated that a longer period for recovery was indispensable.

2.7. Histological assessment of sciatic nerve target muscles post-surgery

The tibialis anterior and gastrocnemius muscles were dissected out bilaterally in accordance with the surgical procedures [21]. The muscles in the nongrafted group were obviously atrophied and fibrotic when compared to the contralateral normal muscles of non-surgical side. While the muscles in the experimental group, the autologous group, and the scaffolding group were much better, with the color of dark red and the texture of softness.

The weights of the gastrocnemius and tibialis anterior muscles on the operated side and the contralateral side were weighed and recorded at 12 weeks postoperatively (Fig. 8a and b). The percentage of wet weight of the gastrocnemius and tibialis anterior muscles were statistically different between all the grafted group and the nongrafted groups. There was no statistical difference between the TENG and the autograft group. Both are superior to the scaffold group. This suggests that the grafting with TENGs or autologous nerve grafts can prevent muscle atrophy and promote muscle recovery.

Masson's trichrome staining showed the muscle fibers dark red and collagen fibers blue. In normal group, the muscle fibers were regular, full, and evenly distributed, with a handful collagen fibers in the muscle interstices and a few small blood vessels. In the TENG and autograft groups, the muscle fibers were relatively full, with a small number of blue-stained collagen fibers and small blood vessels between the muscle bundles. In the scaffold group, the muscle bundles were significantly smaller than those in the normal group. They were atrophied, and large blood vessels and blue-stained collagen fibers were seen between the muscle bundles. In the nongrafted group, the muscle bundles had been significantly atrophied, and the inter-bundles were filled with a large number of collagen fibers (Fig. 8c, e, 8g, 8i, 8k). Morphometric analysis (Fig. 8m, n) showed similar data of the cross-sectional area of muscle fibers and average percentage of collagen fiber area in the TENG and autograft groups, which were superior to animals treated with the scaffold alone. These parameters in non-grafted group were significantly the worst.

After sciatic nerve injury, the target muscle loses innervation, muscle motor function is lost, and neurotrophic atrophy occur simultaneously. Therefore, the regeneration of sciatic nerve axons and reinnervation are directly related to the recovery of the motor endplates of the target muscles. The α-bungarotoxin staining of motor endplates specifically labels nicotinic acetylcholinergic receptors and thus reveals the morphology of the muscle endplates. In the normal muscle, large, round or elliptical endplates were visible, and in the TENG and autologous groups, the endplates were clearly visible. The endplates in the scaffold group were deformed, while in the defect group, the number of endplates was significantly reduced, and they were morphologically striated, with the muscle atrophied.

3. Discussion

Peripheral nerve injuries pose significant challenges in clinical treatment due to their limited intrinsic regenerative capacity [22]. Tissue engineering approaches offer promising solutions by providing biomimetic scaffolds and cell sources to promote nerve regeneration [23]. Despite advancements in surgical techniques and rehabilitation strategies, many patients continue to experience persistent sensory and motor deficits following nerve trauma [3].

SCs play a crucial role in the regeneration and repair of the PNS [24]. Recent advancements in stem cell technologies have offered new avenues for generating engineered therapeutic SCs from various accessible cell sources [25]. SKPs have garnered attention as a potential cell source for tissue engineering due to their accessibility and regenerative potential [26]. Similar work as skin derived precursor SCs-generated acellular matrix modified chitosan/silk scaffolds for bridging rat sciatic nerve gap [27], adult SKP-SCs exhibit superior myelination and regeneration supportive properties [28–31], were reported over one decade ago. In the present work, we investigated the potential roles of SKPs induced neurons and SCs in TENGs to enhance peripheral neuroregeneration for the first time. By inducing SKPs into neurons and Schwann cells *in vitro*, we aimed to harness their regenerative potential for peripheral nerve repair. The TENGs were fabricated using induced SKPs and biocompatible scaffold materials, including chitosan neural conduit and silk fibroin filaments, to mimic the natural microenvironment of nerves. Chitosan served as the neural conduit, providing physical support and guidance for axonal growth [32]. Silk fibroin, known for its mechanical properties and ability to promote cell attachment and proliferation, reinforced the scaffold [33].

Our results demonstrate that TENGs significantly enhance nerve regeneration compared to scaffold control groups, even rivaling the outcomes achieved with autografts, the current gold standard for nerve repair. Histological analysis reveals improved axonal regrowth, myelination, and functional recovery in animals treated with TENGs, indicating their potential for promoting comprehensive nerve repair. Furthermore, immunohistochemical staining confirms the presence of induced neurons and Schwann cells within the regenerated nerve tissue, highlighting the integration of these cells into the host environment. This suggests that the induced cells play a crucial role in facilitating neuroregeneration and functional recovery following nerve injury. Immunohistochemical staining confirmed the presence of induced SKP-neurons and SKP-SCs within the regenerated nerve tissue, suggesting their integration into the host environment. This underscores the crucial role of induced cells in facilitating neuroregeneration and functional recovery following nerve injury.

Isolation and differentiation of SKPs into neurons and SCs are crucial steps in the fabrication of TENGs. Our study successfully induced SKPs into neuronal and Schwann cell lineages, as evidenced by immunocytochemical staining for specific markers such as NF-200, Beta III-tubulin, S100β, and P75. The ability to differentiate SKPs into these cell types provides a valuable cell source for constructing TENGs and promoting peripheral nerve regeneration [34].

The constructed TENGs comprised SKP-induced neurons and SCs

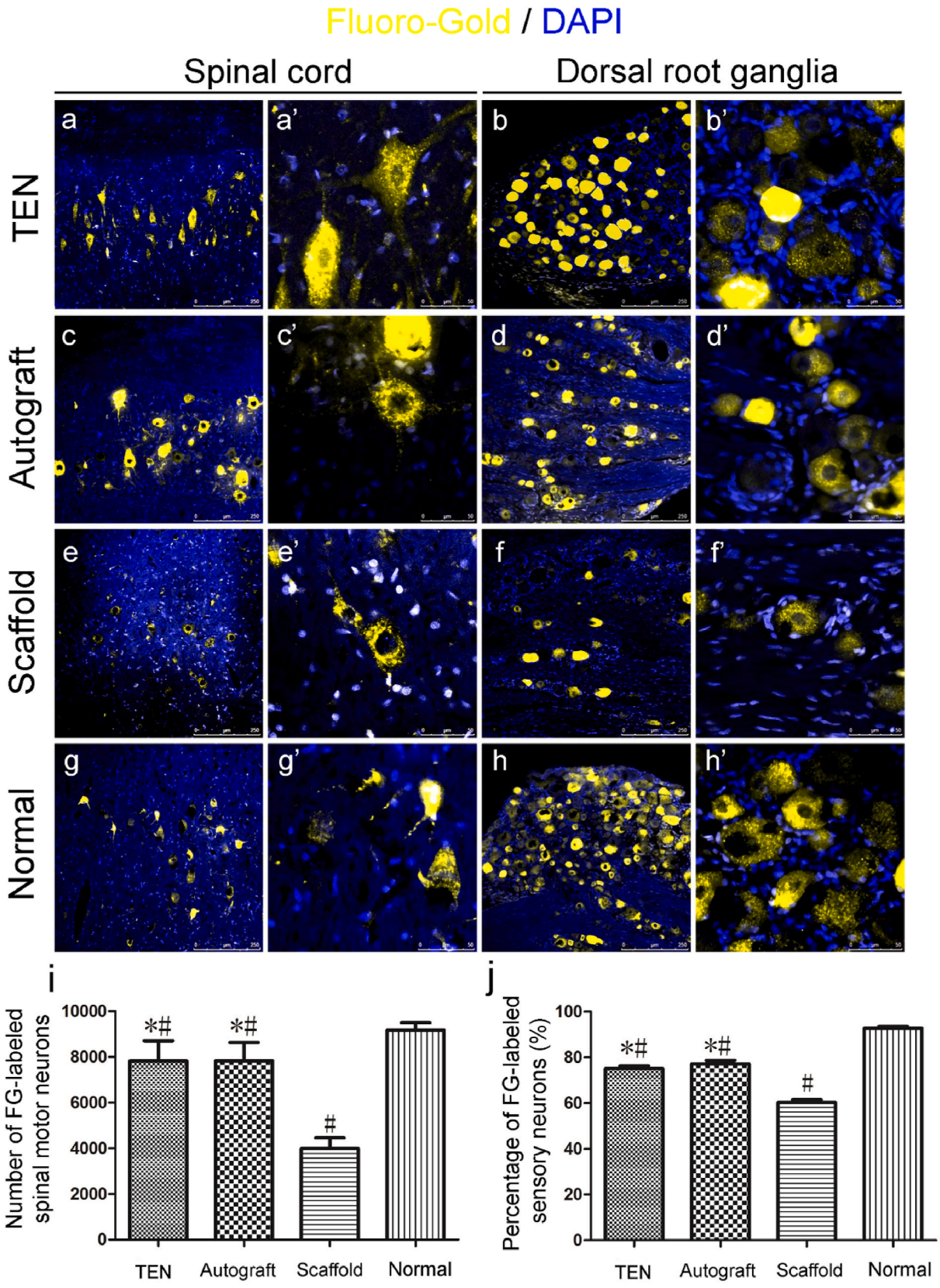

Fig. 6. FluoroGold™ retrograde nerve tracing. Representative fluorescence micrographs following FluoroGold™ (FG) retrograde nerve tracing. FG (gold) retrogradely labeled motor neurons in the spinal cord (a, c, e, g) and sensory neurons in DRGs (b, d, f, h), which double-labeled with DAPI (blue) for clearly showing outlines of the sensory neurons. The high magnifications clearly showed the FG-labeled motor neurons in longitudinal sections of spinal cord (a', c', e', g') and sensory neurons in DRGs (b', d', f', h'), respectively. Scale bar: 250 μm for low magnifications of spinal cord, 50 μm for high magnifications of spinal cord and DRGs. (i, j) Histograms of the number of FG-labeled spinal motor neurons and percentage of FG-labeled sensory DRG neurons were shown and analyzed (n = 3). $^{*}p < 0.05$ versus scaffold group and $^{\#}p < 0.05$ versus normal group.

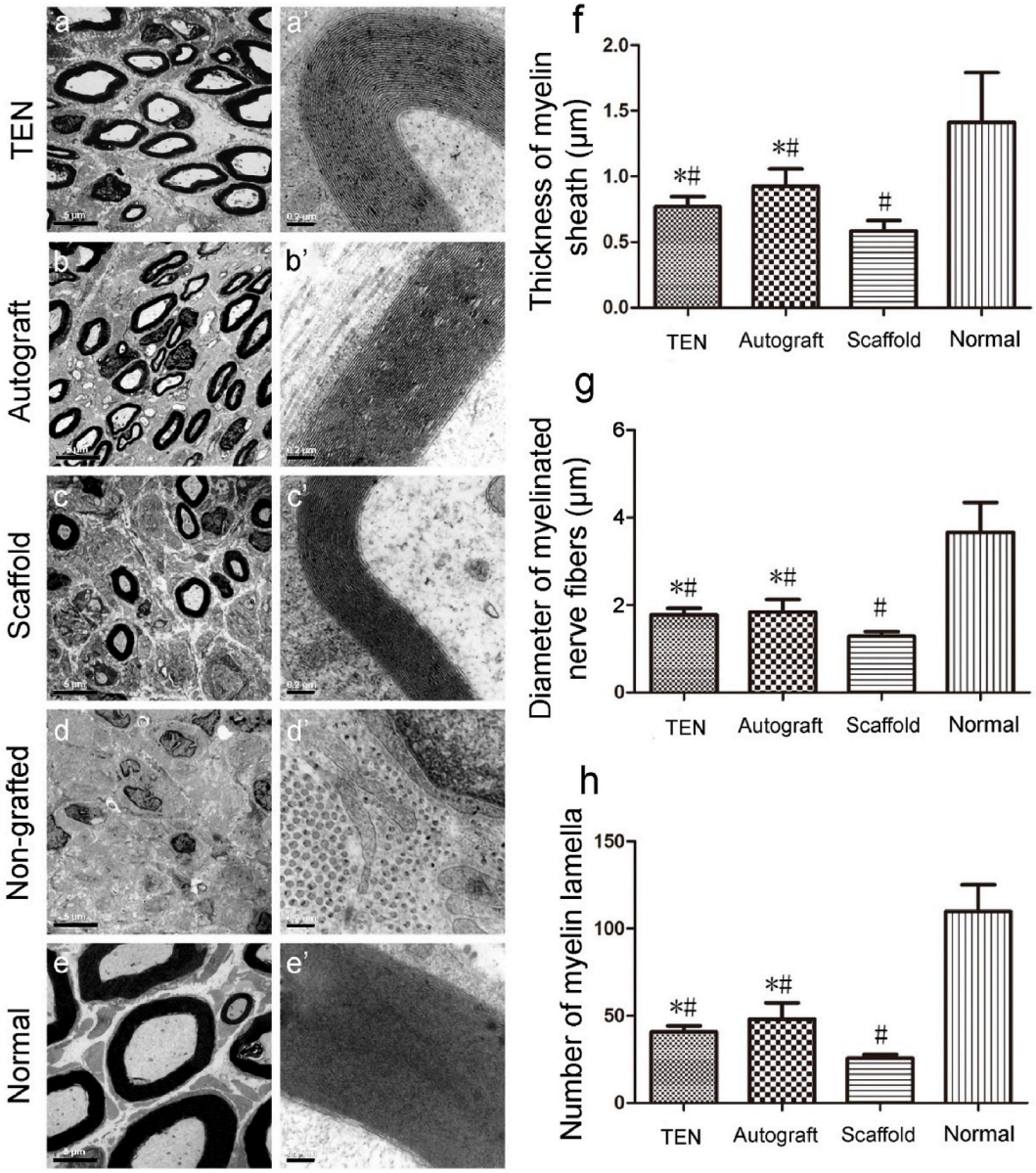

Fig. 7. Histological observation and morphometric analysis of the regenerated nerve. Transmission electron micrographs (a–e) and high magnifications for myelin lamellae (a'-e') are obtained at 12 weeks post-surgery. Scale bar: 5 μm for TEM images and 0.2 mm for myelin lamellae images. Histograms showing the thickness of the regenerated myelin sheath (f), the diameter of regenerated myelinated nerve fibers (g), and the number of regenerated myelin lamella (h). Data are expressed as means ± SD. One-way ANOVA and the post hoc Tukey's *t*-test are used to analyze the data. $^{*}p < 0.05$ versus scaffold group and $^{\#}p < 0.05$ versus normal group.

seeded onto chitosan neural conduits and silk fibroin filaments. Scanning electron microscopy revealed the adhesion of cells to scaffold materials, with a tendency for distribution along the longitudinal axis of the filaments. Immunocytochemical staining confirmed the expression of specific markers by the seeded cells and the presence of extracellular matrix components such as collagen I, collagen IV, and laminin. These results indicate successful integration of cells into the scaffold and the formation of a conducive microenvironment for nerve regeneration. Immediately after nerve injury, SKP-Neurons and SKP-SCs could be expected to respond to signals released from the damaged tissue, such as growth factors and cytokines, which initiate the regenerative process. SKP-SCs, similar to native Schwann cells, may associate with the damaged axons and provide a supportive environment for axonal regeneration by releasing neurotrophic factors [6]. SKP-Neurons might integrate into the neural network, potentially replacing lost neurons or supporting the survival of injured ones. SKP-SCs are known [34] to secrete angiogenic factors that can stimulate the formation of new blood vessels, which is essential for supplying oxygen and nutrients to the regenerating nerve tissue. The presence of new blood vessels also facilitates the removal of waste products and immune cells from the injury site, promoting a healthier environment for regeneration. SKP-SCs can influence the immune response by releasing cytokines that modulate inflammation. They can help to resolve the initial inflammatory response post-injury, which is crucial for preventing excessive scarring and damage. These cells might also recruit immune cells like macrophages to the injury site, which can clear debris and release growth factors that support regeneration. SKP-SCs and SKP-neurons could contribute to the formation of a permissive extracellular matrix that guides axonal growth and provides structural support for tissue repair. By differentiating into functional neural cells, these SKP-derived cells could help restore the neural functions and improve the overall tissue architecture. SKP-Neurons and SKP-SCs might release neuroprotective factors that protect resident neurons from secondary injury, promoting their survival and enhancing the overall regenerative capacity of the

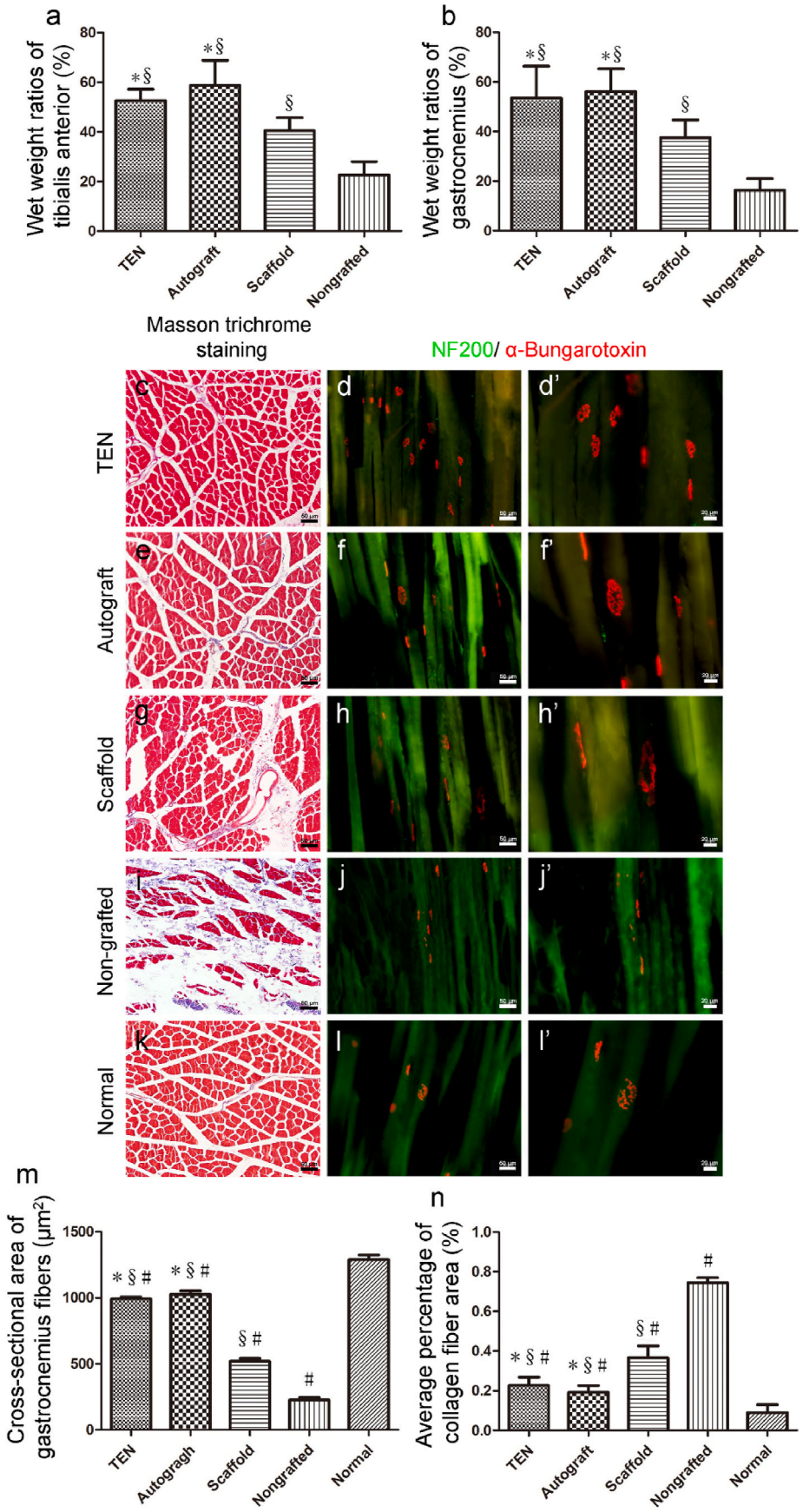

(caption on next page)

Fig. 8. Histological observation and morphometric analysis of the target muscles. (a, b) Histograms showing the wet weight ratio of total anterior tibialis and gastrocnemius muscle, and the cross-sectional area of gastrocnemius muscle fibers. Data are expressed as means ± SD. $^{*}p < 0.05$ versus scaffold group, $^{\S}p < 0.05$ versus non-grafted group. (c, e, g, i, k) Masson's trichrome staining images are obtained at 12 weeks post-surgery, of the sectioned gastrocnemius muscle on the injured side in TENG (c), autograft (e), scaffold (g), non-grafted groups (i) and the contralateral uninjured side (k, normal), respectively. Scale bar, 50 mm. Photomicrographs (d, f, h, j, l and d', f', h', j', l') of longitudinal sections of gastrocnemius muscles at the injured side after α-bungarotoxin staining of motor endplates (red) and NF200 (green) positive regenerated axons are obtained in three nerve grafting groups, nongrafted group and the contralateral uninjured side muscle at 12 weeks. Scale bar: 50 μm for low magnification images, and 20 μm for high magnification images. Histograms showing the cross-sectional area of gastrocnemius muscle fibers (m) and average percentage of collagen fiber area (n). Data are expressed as means ± SD. $^{*}p < 0.05$ versus scaffold group, $^{\S}p < 0.05$ versus non-grafted group and $^{\#}p < 0.05$ versus normal group.

nerve. As part of the tissue repair process, SKP-neurons could potentially form new synaptic connections with other neurons or target tissues, aiding in the recovery of nerve function. SKP-SCs could differentiate into myelin-producing cells, which are essential for the remyelination of demyelinated axons, leading to improved nerve conduction velocity and function. The integration of SKP-SCs and SKP-neurons with endogenous neural cells, including neurons, resident SCs, and immune cells, is critical for orchestrating a coordinated regenerative response. The long-term presence and activity of SKP-SCs and SKP-neurons could contribute to sustained functional recovery by continuously providing trophic support and participating in the reorganization of the neural circuitry.

Behavioral tests and neuro-electrophysiological analyses demonstrated improved sciatic nerve functional recovery in animals treated with TENGs compared to scaffold control groups. The CatWalk™ gait analysis system revealed better SFI values in the TENG and autograft groups, indicating enhanced motor function. Similarly, CMAP recordings and MCV calculations showed superior outcomes in the TENG and autograft groups, suggesting improved nerve conduction.

Tracing of seed cells *in vivo* revealed the survival of SKP-induced neurons and Schwann cells at the implantation site, indicating their potential role in promoting nerve regeneration. Cryo-longitudinal-section and immunofluorescence labeling further demonstrated enhanced axon regeneration in animals treated with TENGs compared to scaffold controls. Histological evaluation of regenerated nerves showed increased density of myelinated nerve fibers in the TENG and autograft groups, indicating successful axonal regrowth. To provide a comprehensive understanding of the host-graft relationship, the interactions between the transplanted cells and the host tissue, including immune responses, angiogenesis, and the formation of the extracellular matrix should be investigated. The SKP-SCs and SKP-Neurons exhibit neuroprotective effects, such as the secretion of neurotrophic factors or the modulation of the inflammatory response. The potential complications associated with the transplantation of SKP-SCs and SKP-Neurons, such as tumorigenicity, immune rejection, or malfunction, along with mechanisms to mitigate these risks should be further explored. The optimization of transplantation techniques the development of strategies to enhance cell survival and integration, and the exploration of combinatorial therapies involving SKP-SCs and SKP-Neurons will be developed in future.

FG tracing demonstrated superior reconstruction of neural pathways and axonal transportation in animals treated with TENGs compared to scaffold controls. Ultrastructural assessment via TEM revealed the formation of myelinated nerve fibers with electron-dense myelin sheaths in the TENG and autograft groups. Morphometric analysis showed comparable parameters of myelin sheath thickness, diameter of myelinated nerve fibers, and number of myelin lamellae between the TENG and autograft groups, indicating successful nerve regeneration.

Histological assessment of target muscles post-surgery showed improved muscle morphology and reduced fibrosis in animals treated with TENGs compared to scaffold controls. Masson's trichrome staining revealed increased muscle fiber density and decreased collagen deposition in the TENG and autograft groups, indicating better muscle regeneration. α-Bungarotoxin staining of motor endplates showed preserved morphology and increased number of endplates in animals treated with TENGs, suggesting improved neuromuscular junction integrity. The α-bungarotoxin staining of motor endplates revealed that in the TENG and autologous groups, the endplates were clearly visible, suggesting that the grafting with TENGs or autologous nerve grafts can promote the regeneration of sciatic nerve axons and reinnervation, which are directly related to the recovery of the motor endplates of the target muscles [35].

The study highlights the promise of SKP-induced neurons and SCs in TENGs. However, several aspects warrant further exploration. ①Fine-tuning the differentiation process and scaffold design to enhance cell survival and integration. ②Investigating the long-term effects of TENGs, including functional recovery and stability. Ensuring long-term survival, integration, and functionality of transplanted SKPs within the host tissue is critical. SKPs must interact with the existing cellular environment and contribute to tissue repair over extended periods. ③Clinical trials are necessary to validate the efficacy and safety of TENGs in human patients. Rigorous testing is essential to minimize adverse effects and maximize therapeutic benefits.

Our findings underscore the potential of SKP-induced neurons and SCs in tissue-engineered nerve grafts as a promising approach for enhancing peripheral nerve regeneration. Leveraging endogenous cell sources and biomimetic scaffolds offers a feasible strategy for clinical translation in the treatment of peripheral nerve injuries. Despite these promising results, challenges remain in translating SKP research to clinical applications. The density of regenerated nerve fibers was significantly higher in both the TENG and autograft groups than in the scaffold group, all the grafted groups did not catch up with the normal control, indicating that further improvements are needed. In future research, efforts should focus on optimizing the survival, differentiation, and integration of SKPs within tissue-engineered constructs to enhance their therapeutic potential. Additionally, exploring combinatorial approaches involving growth factors, gene therapy, and electrical stimulation may further augment nerve regeneration outcomes [4,36,37]. The development of effective strategies for peripheral nerve repair holds promise for improving the quality of life for patients with nerve injuries [38,39].

The regenerative microenvironment is a crucial aspect of tissue engineering and nerve regeneration [40,41]. It encompasses a complex interplay of various factors that facilitate the repair and regrowth of damaged nerves. The traditional triad of tissue engineering-scaffold, cells, and growth factors-is essential, but the regenerative microenvironment adds another layer of complexity and specificity. The microenvironment is rich in signaling molecules such as cytokines, chemokines, and extracellular matrix (ECM) components [42]. These molecules guide cell migration, proliferation, and differentiation. The availability of oxygen can influence the behavior of cells in the microenvironment. Hypoxia (low oxygen levels) can stimulate certain regenerative processes, while normoxia (normal oxygen levels) might be necessary for optimal cell function [43]. Adequate supply of nutrients like glucose, amino acids, and vitamins is essential for cell survival and function. The microenvironment must facilitate efficient nutrient transport and metabolism. Mechanical forces, such as tension and compression, can influence cell behavior and gene expression. The stiffness and topography of the scaffold can mimic the natural tissue environment and guide nerve regeneration [44]. The initial inflammatory response following injury is crucial for clearing debris and initiating the regenerative process. However, prolonged inflammation can be

detrimental, so the microenvironment must balance pro- and anti-inflammatory signals [45]. Cells like SCs in the peripheral nervous system and astrocytes in the central nervous system play a supportive role in nerve regeneration. They secrete growth factors and provide structural support. The ECM provides a physical scaffold and biochemical signals that influence cell behavior [46]. Its composition and organization can be tailored to support nerve regeneration. The scaffolds mimic the natural ECM to support cell attachment, migration, and differentiation. It should be biocompatible, biodegradable, and have mechanical properties that match the target tissue. The microenvironment's mechanical cues and ECM composition guide the design of the scaffold [34]. The presence of specific cell types, such as stem cells or Schwann cells, can be manipulated to enhance the regenerative potential of the microenvironment. The microenvironment's molecular signals and mechanical properties influence cell behavior, such as migration, proliferation, and differentiation [6]. The delivery and release of growth factors must be carefully controlled to mimic the natural regenerative process. The microenvironment's inflammatory state and glial cell activity can modulate the effectiveness of growth factors. The interplay between scaffolds, cells, and growth factors is dynamic. For example, the scaffold can influence the spatial distribution of cells and growth factors, while cells can modify the scaffold through secretion of ECM components and growth factors. The regenerative microenvironment is a multifaceted and dynamic system that plays a pivotal role in nerve regeneration. Understanding and manipulating this microenvironment can significantly enhance the outcomes of tissue engineering strategies aimed at nerve repair. Further research is needed to fully elucidate the complex interactions and to develop effective therapeutic strategies.

4. Conclusion

In conclusion, our study demonstrates the potential of SKP-induced neurons and SCs in TENGs for enhancing peripheral neuroregeneration. The successful fabrication and characterization of TENGs, coupled with improved functional and histological outcomes, highlight the promising prospects of this approach for clinical translation in the treatment of peripheral nerve injuries. The use of SKPs in nerve regeneration offers a promising alternative to traditional cell sources due to their accessibility, differentiation potential, and unique properties. Our findings underscore the potential of SKP-induced neurons and SCs in TENGs as a promising approach for enhancing peripheral nerve regeneration. The ability to harness endogenous cell sources and biomimetic scaffolds offers a feasible and scalable strategy for clinical translation in the treatment of peripheral nerve injuries. However, further optimization and characterization of these engineered constructs are warranted to maximize their clinical applicability and efficacy. Further optimization and validation of TENGs are warranted to maximize their efficacy and applicability in clinical practice.

5. Materials and methods

5.1. Animals

Newborn (1–3 d) and adult (weight 220 g–250 g) Sprague Dawley (SD) rats were provided by the Experimental Animal Centre of Nantong University (License No. SYXK (Su) 2017-0046). All experimental protocols were approved by the Administration Committee of Experimental Animals, Jiangsu Province, China, in accordance with the guidelines of the Institutional Animal Care and Use Committee, Nantong University, China (Inspection No: 20190225-004).

5.2. Isolation of SKPs and the induced differentiation into SKP-neurons and SKP-SCs

To isolate and purify SKPs from the skin of wild type and green fluorescent protein (GFP) transgenic newborn rats, an optimized protocol was carried out as described previously [19,47]. One day old SD rats were taken and the skin was defatted with 75 % alcohol. The rats were transferred to a sterile ultra-clean table in the cell culture room, and 2 cm^2 of skin was cut with ophthalmic scissors and placed into pre-cooled DMEM/F12 (3:1) medium, and all the subcutaneous fat, blood vessels and other connective tissue layers were removed. The processed skin was transferred into a centrifuge tube and the skin was cut into skin pieces of 1 mm^2 size. After rinsing twice with PBS, 3 times the volume of skin was added with pre-warmed collagenase XI (Sigma, cat. no. C9407), and placed in a 37 °C, CO_2 cell culture incubator for digestion for 45–60 min, during which time it was blown up every 15 min, and when the liquid was milky and/or coeliacal in consistency, and the skin morphology was completely disappeared, 10–15 ml of the digestive termination solution was added. Filter through a 400-mesh screen and rinse with 15 ml of DMEM/F12 (3:1) and collect all the filtrate by centrifugation at 1200 rpm for 7 min. The supernatant was discarded and the cells were resuspended by adding 2 ml of DMEM/F12 (3:1) and counted. The cells were cultured with "SKPs proliferation medium" at a cell density of 10^5/ml for 1–3 weeks. The "SKPs proliferation medium" which contained DMEM/F12 (3:1), 1 % penicillin/streptomycin (Thermo Fisher Scientific, Shanghai, China), 2 % B27 supplement (Invitrogen, Carlsbad, CA, USA), 20 ng/ml EGF, and 40 ng/ml FGF-2 (BD Bioscience, San Diego, CA, USA), 1 μg/ul Fungizone (Invitrogen, cat. no. 15290-018) were changed every 3 days. Transfer the medium with suspended SKP spheres into a centrifuge tube and centrifuge at 1000 rpm for 3–5 min. After discarding the supernatant, collagenase XI was added and digested at 37 °C. The cells were allowed to dissociate into single cells, and the digestion was terminated and centrifuged.

Differentiation towards neurons: After centrifugation, the cells were resuspended in DMEM/F12 (3:1) medium containing 7 % fetal bovine serum (FBS), and then seeded into a poly-D-lysine and laminin coated dish containing DMEM/F12 (3:1) medium containing 7 % FBS at a density of 10^6/ml. bFGF was added at a rate of 40 ng/ml, and then mixed well, and then placed at 37 °C in an incubator with 5 % CO_2, and cultured for 3 days. Then, the medium was discarded and replaced with "SKP-neurons differentiation medium" to continue the culture, and then the medium was changed every 3 days to wait for the appearance of neuron-like long axonal cells. It takes 2–3 weeks. "SKP-neurons differentiation medium" contained DMEM/F12 (3:1), 1 % penicillin/streptomycin, 7 % FBS, 10 ng/ml BDNF，50 ng/ml NGF， and 10 ng/ml NT-3.

Differentiation towards SCs: After centrifugation, cells were resuspended with SKP medium, then seeded at a cell density of 10^6/ml into SKP medium-containing coated petri dishes, and cultured at 37 °C in a 5 % CO_2 incubator for three days. Then, the medium was discarded and replaced with "SKP-SCs differentiation medium" for further cultivation, and the medium was changed every three days thereafter. The "SKP-SCs differentiation medium" which contained DMEM/F12 (3:1), 1 % penicillin/streptomycin, 5 % FBS, 2 % B27 supplement, 20 ng/ml EGF, and 40 ng/ml FGF-2, 1 μg/ul Fungizone Antimycotic. The SKP-SCs were allowed to appear and gradually proliferate into colonies with high purity. Use a 1 mm^2 sized sterilized filter paper sheet, immersed in 0.125 % trypsin, to carefully digest SKP-SCs colonies under a microscope, carefully collect the cells and plant them in a new coated petri dish, and continue to expand the culture with "SKP-SCs culture medium", which consist of DMEM/F12 (3:1) containing 0.1 % penicillin/streptomycin, 5 μm forskolin, 50 ng/ml heregulin-1β (R&D Systems, cat. no. 377-HB), 2 % N2 supplement (Invitrogen, cat. no. 17502), 5 % FBS. After 2–3 times in this way, SKP-SCs cells were evenly spread on the bottom of the dish and passaged every 2–3 generations according to the growth, which took 2–3 weeks.

5.3. Construction of SKP-TENGs

Rats were deeply anaesthetized by an intraperitoneal injection of compound anesthetic (magnesium sulfate 2.12 g, sodium pentobarbital 886 mg, ethanol 14.25 ml, and propylene glycol 33.8 ml in 100 ml) [6]. The TENG is consist of chitosan neural conduit (i.d. 2.0 mm, Chinese patent ZL 0110820.9A) inserted with about 120 silk fibroin fibers (12 mm long, diameter 8 μm) were soaked in the poly-D-lysine and laminin coated solutions for 24 h [19]. The chitosan neural conduit and SF fibrous fillers were prepared as described previously [6]. Tissue-engineered neural conduits (containing silk fibroin fibers) were soaked in tissue-engineering coating solution, which contained 0.2 μg/ml poly-D-lysine and 0.02 μg/ml laminin in PBS at 4 °C overnight, and then washed 3–5 times in PBS before being ready for use.

The SKP-SCs and SKP-Neurons were digested and resuspended at a ratio of 20:1 and mixed, counted and adjusted to 2×10^4/μl, and then planted into each tissue-engineered conduit according to the standard of 50 μl for each tissue-engineered nerve (10 mm) in order, and then placed the tissue-engineered nerves into the matched petri dishes carefully. Place the tissue-engineered nerves carefully into the matched culture dishes and incubate them at 37 °C, 5 % CO_2 incubator for 3 h. After the cells were attached to the wall, add the cell co-culture stimulation medium, which contained DMEM/F12 (3:1), 1 % penicillin/streptomycin, 15 % FBS, 50 ng/ml ascorbic acid, 10 ng/ml BDNF , 50 ng/ml NGF , and 10 ng/ml NT-3, and incubate them at 37 °C, 5 % CO_2 incubator, protected from light for 14 days, and change the medium every two days during the period of incubation. After the TENGs culture was finished, they were immersed in 0.01M PBS and stored at 4 °C.

5.4. Immunocytochemical staining

After SKPs were centrifuged, SKP medium was resuspended and counted, seeded at a density of 15–20 cell spheres/15 mm round slides into 6-well plates containing 15 mm round slides, placed in a 37 °C, 5 % CO_2 incubator, and when about 20 % of the area of each cell sphere was affixed to the round slides, the medium was discarded, rinsed three times with PBS, fixed in 4 % paraformaldehyde (PFA) for 20 min, soaked in PBS, and preserved at 4 °C for spare use. The cells were fixed in 4 % PFA for 20 min. This process was about 30 min.

Same as the steps for SKPs, SKP-SCs and SKP-Neurons were centrifuged and resuspended respectively and planted into round slides at appropriate density, and cultured in the corresponding medium for 24–48 h, then the medium was discarded, rinsed in PBS for 3 times, fixed in 4 % PFA for 5min, soaked in PBS, and stored at 4 °C for spare use.

The fixed round slide was incubated with the required primary antibodies at 4 °C overnight (Mouse anti-vimentin antibody, Rabbit anti-versican 1 antibody, Mouse anti-vimentin antibody, Rabbit anti-versican 1 antibody, Mouse anti-fibronectin antibody, Rabbit anti-nestin antibody, Rabbit anti-αSMA antibody, Mouse anti-SCA1 antibody, Mouse anti-P75 antibody, Rabbit anti-S100 antibody, Mouse anti-NF 200 antibody, Rabbit anti-beta III Tubulin antibody). Then the secondary antibodies from the corresponding sources to the primary antibody (Goat anti-mouse IgG-Alex-488 and Donkey anti-rabbit IgG-Cy3) were added, incubate at room temperature for 2 h. After washing three times, seal the slices by carefully adding drops of fluorescent sealing solution and place them under a fluorescent orthostatic microscope for observation, photographing and recording.

The TENGs that were cultured were washed in PBS, immersed in 4 % PFA for 15 min, washed in PBS for 3 times, and stored at 4 °C. The silk fibroin filaments in the fixed spare tissue-engineered nerves were withdrawn, washed once with PBS. The required primary antibodies were added, respectively (Mouse anti-P75 antibody, Rabbit anti-S100 antibody, Mouse anti-NF 200 antibody, Rabbit anti-beta III Tubulin antibody, Mouse anti-fibronectin antibody, Rabbit anti-laminin antibody, Mouse anti-collagenIantibody, Rabbit anti-collagen IV antibody). After washing three times, add the secondary antibody of the source corresponding to the primary antibody (Goat anti-mouse IgG-Alex-488 and Donkey anti-rabbit IgG-Cy3) corresponding to the primary antibody, incubate at 4 °C overnight. After washing three times, the fluorescent sealing solution was carefully added dropwise and sealed (to ensure that there were no air bubbles), placed in a laser confocal microscope for observation, photographing and recording.

5.5. Scanning electron microscope (SEM)

The new tissue-engineered nerves completed by chaperoning were fixed in 4 % glutaraldehyde for 30 min, and washed by PBS for 3 times, each time for 10 min; 1 % osmium acid (OsO_4) was fixed in light protection for 2 h, and washed by PBS for 3 times, each time for 10 min (osmium acid fixation and washing should be carried out in a ventilated kitchen); the nerves were dehydrated with a gradient of 30 %, 50 %, 70 %, 80 %, and 95 % in turn, each time for 10 min, and finally dehydrated twice with Anhydrous ethanol dehydration twice, each time 10min; after evaporation of the remaining anhydrous ethanol in the ventilated kitchen, the tissue-engineered nerves were dissected, and the silk firoin filaments and chitosan neural conduit were fixed on the copper block platform of the scanning electron microscope loader, respectively. Afterward, samples processed were dried in a freeze drier (Hitachi, ES-2030, Japan) and coated with platinum using a JEOL JFC-110E Ion Sputter, followed by observation under a Philips XL-30 scanning electron microscope (Eindhoven, the Netherlands).

5.6. Sciatic nerve surgical procedure

All animals were deeply anaesthetized. The skin and muscle were incised to expose the sciatic nerve at the left mid-thigh. An 8-mm segment of the sciatic nerve was resected to form a 10 mm gap following slight retraction of the nerve stumps. The nerve stumps on both sides were inserted into the lumen of 12-mm long TENG about 1 mm. Tissue-engineered nerves, severed horizontally flipped sciatic nerves (i.e., the distal and proximal ends of the cut sciatic nerves were switched) and chitosan conduits were sutured to the outer membrane of the nerve stumps with 8/0 medical micro sutures, respectively, and each group of nerves was restored to its original position, and each layer of tissue was sutured sequentially, and the skin was sutured. In the non-grafted group, the sciatic nerve was excised and the severed nerve defect was left without treatment, and the layers of tissue and skin were sutured directly. The sutured wounds were sterilized with iodine povidone, and the groups were labeled and kept in separate cages. The animals were kept in a constant temperature and humidity environment with 12 h of light/dark cycle per day, and were allowed to drink and feed freely.

5.7. Animal behavioral analysis

The CatWalk XT 9.0 gait analysis system was used to assess motor functional recovery. At 4, 8 and 12 weeks after nerve grafting, the animals (n = 10) in 3 groups were placed on the right side of a runway consisting of a glass surface and black plastic walls. The animals were motivated to traverse the runway toward the left end where food pellet rewards were located, and the dynamic process of rats was recorded. The scale categorizes a combination of posture, hind limb movements, hind limb force, and joint motion. The sciatic function index (SFI) value was calculated by the formula: SFI = 109.5(ETS-NTS)/NTS-38.3(EPL-NPL)/NPL+13.3(EIT-NIT)/NIT-8.8, where TS is the total toe spread, IT is the intermediate toe spread, PL is the footprint length, N refers to the contralateral uninjured (normal) side, and E refers to the injured side.

5.8. Electrophysiological test

At 12 w after surgery, all rats in each group were anaesthetized by intraperitoneal injection with the same dose as above, and nerve

electrophysiology of the injured side was performed on TENG, autograft, scaffold groups, and that of the contralateral uninjured side. The nerves at both ends of the grafts were carefully separated with a glass split-needle, and the compound muscle action potentials (CMAPs) were recorded according to Suzuki's method, with the following specific steps: the recording electrodes were inserted into the muscle belly of the target muscle (gastrocnemius muscle), the interfering electrodes were clamped on the incised skin, and the stimulating electrodes were placed on the proximal and distal ends of the grafts, and the stimulating electrodes were clicked on the instrument to stimulate the nerve grafts. The stimulating electrode was placed proximal to the nerve graft and distal to the distal end of the nerve graft in turn, the nerve was stimulated by clicking the instrument, and the amplitude and latency of CMAPs and the distance between the two electrodes were recorded. The contralateral uninjured side of the nerve was stimulated in the same way at the corresponding proximal and distal nerve trunks and the above data were recorded. Conduction velocity = distance between proximal and distal electrodes/(proximal CMAP latency - distal CMAP latency).

5.9. FG retrograde tracing assay

At 12 w postoperatively, three rats were randomly selected from each group and anaesthetized by intraperitoneal injection. The sciatic nerve on the operated side was surgically exposed in TENG, autograft, scaffold groups. The distal end of each graft was made to expose the distal sciatic nerve. The contralateral uninjured sciatic nerve was exposed in the corresponding position. Use tissue forceps to clamp the distal sciatic nerve at the distal end of the bridging material, inject 10 μl of FG into the outer membrane of the sciatic nerve at the injury site with a micro-syringe, close the incision sequentially, and suture the skin. After two weeks, the grafts were taken after 4 % PFA perfusion. The sciatic nerve was retrograded to find the dorsal root ganglions (DRGs) of the L4, L5 and L6 segments, the vertebral plate was opened, and the lumbar bulging part of the spinal cord (i.e., the L4, L5 and L6 segments of the spinal cord) was cut out, and the spinal cord and the DRGs were postfixed in 4 % PFA (post fixation time was 6–8 h). The sectioning procedure was the same as in the previous chapter, the spinal cord was cut longitudinally in the ventral-dorsal direction in the lumbar expansion direction with a thickness of 25 μm, and the DRGs were cut longitudinally with a thickness of 10 μm. The slices were counted under an orthogonal fluorescence microscope, and observed and photographed under a laser confocal microscope.

5.10. Tissue sample processing

After the anaesthetization, the animal skin of the abdominal wall and the peritoneum were opened sequentially, a perfusion needle was inserted retrogradely into the ascending aorta from the inter-ventricular region. The right auricle was cut and saline perfusion was performed; after the liver was discolored and the blood in the mesenteric vessels disappeared, the perfusion was changed to 4 % PFA. When the muscles of the lower limbs were rigid and the tail was stiff and erect, the perfusion was satisfactory. The required nerve and muscle tissues were obtained and post-fixed in 4 % PFA solution.

5.11. Histological assessments and morphometric analysis of regenerated nerves

The transverse section of the regenerated nerve in the distal end was subjected to Meyer's modified trichrome staining, immunofluorescence staining, and transmission electron microscopy as described previously [6]. Meyer's modified trichrome staining was conducted before visualization and photography under light microscopy (Axio Imager 2, ZEISS). For immunofluorescent double-staining, rabbit anti-S100β polyclonal antibody (1:50 dilution) and mouse anti-neurofilament-200 (NF200) monoclonal antibody (1:200 dilution, both antibodies were from Sigma) were applied to nerve sections to allow incubation at 4 °C overnight, followed by further reaction with the secondary antibody (Goat anti-Mouse IgG-Alex-488, 1:500 and Donkey anti-Rabbit IgG-Cy3, 1:1000) at 4 °C overnight, and nerve sections were observed under a confocal laser scanning microscope (TCS SP2, Leica). Images were acquired under a fluorescence microscopy (AxioImager M2, Zeiss).

5.12. Transmission electron microscope (TEM)

The anaesthesia, perfusion and sampling steps of rats were the same as above, and the perfusion fluid was changed to a mixture of 1 % PFA and 1.25 % glutaraldehyde perfusion fluid. Each nerve tissue (bridging the distal sciatic nerve of each material and the normal sciatic nerve tissue of the defect group in the corresponding position) was trimmed to 1.5 mm*1.0 mm*1.0 mm size nerve. The tissues were sequentially immersed in pre-cooled glutaraldehyde fixation and 1 % osmium acid fixation. The nerve tissues were sequentially stained with uranyl acetate block, dehydrated with gradient ethanol, embedded with Epon812 epoxy resin, positioned in semi-thin sections, and finally subjected to ultrathin sectioning of the tissues at 70 nm, and the transverse structure of the nerves was observed under transmission electron microscope after routine lead citrate re-staining and photographed for recording.

The distal nerve trunk of bridge was collected, post-fixed in 4 % glutaraldehyde, and embedded in Epon 812 epoxy resin (Sigma) [48]. Ultrathin sections were conducted and stained with lead citrate and uranyl acetate. The morphology of regenerating nerves was observed under a transmission electron microscope (JEOL Ltd., Tokyo, Japan). The 3 random fields with low magnification per animal were used for myelin sheath thickness statistics. The 5 random fields with high magnification per animal were selected for myelin sheath layers count.

5.13. Histological assessments and morphometric analysis of target muscles

The percentage of wet weight of the target muscle was calculated according to: (weight of the muscle on the operated side/contralateral healthy muscle) × 100 %. Followed by trimming and fixing in 4 % PFA, the mid-belly of the gastrocnemius muscles was cut into transverse sections that underwent Masson's trichrome staining and photography by light microscopy. The longitudinal sections were subjected to double-staining with α-bungarotoxin and mouse anti-NF200 monoclonal antibody followed by photography under a Zeiss Inverted Fluorescence Microscope (AxioImager M2, Zeiss).

5.14. Statistical analysis

The data were presented as means ± standard deviation (SD). One-way analysis of variance (ANOVA) was used for multiple comparisons (Tukey's post hoc test) among groups. Statistical analysis was performed by using Graph-Pad Prism 10.0 software (GraphPad Software Inc., La Jolla, CA, USA). A p-value< 0.05 was considered as statistically significant.

Ethics statement

Adult female Sprague-Dawley (SD) rats about 220∼250 g were acquired from the Experimental Animal Center of Nantong University (License No. SYXK (Su) 2017-0046). All experimental protocols were approved by the Administration Committee of Experimental Animals, Jiangsu Province, China, in accordance with the guidelines of the Institutional Animal Care and Use Committee, Nantong University, China (Inspection No: 20190225-004).

CRediT authorship contribution statement

Qi Guo: Writing – original draft, Visualization, Validation, Project

administration, Methodology. **Hui Zhu:** Writing – review & editing, Writing – original draft, Validation, Resources, Project administration, Methodology, Investigation, Funding acquisition, Formal analysis, Data curation. **Xi Xu:** Project administration, Methodology, Investigation, Formal analysis, Data curation. **Tianyi Huang:** Visualization, Validation, Investigation, Formal analysis, Data curation. **Yulin Pan:** Visualization, Validation, Project administration, Methodology, Investigation, Formal analysis. **Xiaosong Gu:** Supervision, Funding acquisition, Conceptualization. **Shusen Cui:** Writing – review & editing, Supervision, Conceptualization. **Chengbin Xue:** Writing – review & editing, Writing – original draft, Visualization, Validation, Supervision, Software, Resources, Project administration, Methodology, Investigation, Funding acquisition, Formal analysis, Data curation, Conceptualization.

Declaration of competing interest

The authors declare that they have no known competing financial interests or personal relationships that could have appeared to influence the work reported in this paper.

Data availability

Data will be made available on request.

Acknowledgements

This work was graciously supported by National Key R&D Program of China (2022YFC2409800, 2022YFC2409802), National Natural Science Foundation of China (Grant No. 82172104), Natural Science Foundation of Jiangsu Province (BK 2024023679), Jiangsu Provincial Research Hospital (YJXYY202204, YJXYY202204-ZD04), Jiangsu Provincial Key Medical Center, Jiangsu Provincial Medical Innovation Center (CXZX202212), Jiangsu Provincial Medical Key Discipline (ZDXK202240), the Priority Academic Program Development of Jiangsu Higher Education Institutions (PAPD), and Technology Project of Nantong (MS22022008).

References

[1] R. Sun, Y. Lang, M.W. Chang, M. Zhao, C. Li, S. Liu, B. Wang, Leveraging oriented lateral walls of nerve guidance conduit with core–shell MWCNTs fibers for peripheral nerve regeneration, Adv. Healthcare Mater. 13 (13) (2024) 2303867.
[2] W. Zhou, M.S.U. Rahman, C. Sun, S. Li, N. Zhang, H. Chen, C.C. Han, S. Xu, Y. Liu, Perspectives on the novel multifunctional nerve guidance conduits: from specific regenerative procedures to motor function rebuilding, Adv. Mater. 36 (14) (2024) 2307805.
[3] X. Gu, Biodegradable materials and the tissue engineering of nerves, Engineering 7 (12) (2021) 1700–1703.
[4] N. Zhu, Y. Zhuang, W. Sun, J. Wang, F. Wang, X. Han, Z. Han, M. Ni, W. Cui, Y. Qiu, Multistructured hydrogel promotes nerve regeneration, Materials Today Advances 21 (2024) 100465.
[5] H. Wang, S. Huddleston, J. Yang, G.A. Ameer, Enabling proregenerative medical devices via citrate-based biomaterials: transitioning from inert to regenerative biomaterials, Adv. Mater. 36 (6) (2023) 2306326.
[6] C. Xue, H. Zhu, H. Wang, Y. Wang, X. Xu, S. Zhou, D. Liu, Y. Zhao, T. Qian, Q. Guo, Skin derived precursors induced Schwann cells mediated tissue engineering-aided neuroregeneration across sciatic nerve defect, Bioact. Mater. 33 (2024) 572–590.
[7] H.-S. Kim, J.Y. Kim, C.L. Song, J.E. Jeong, Y.S. Cho, Directly induced human Schwann cell precursors as a valuable source of Schwann cells, Stem Cell Res. Ther. 11 (1) (2020) 257.
[8] A.D. Jerome, A.R. Sas, Y. Wang, L.A. Hammond, J. Wen, J.R. Atkinson, A. Webb, T. Liu, B.M. Segal, Cytokine polarized, alternatively activated bone marrow neutrophils drive axon regeneration, Nat. Immunol. 25 (6) (2024) 957–968.
[9] S.M. Hosseini, B. Borys, S. Karimi-Abdolrezaee, Neural stem cell therapies for spinal cord injury repair: an update on recent preclinical and clinical advances, Brain 147 (3) (2024) 766–793.
[10] S. Brambilla, M. Guiotto, E. Torretta, I. Armenia, M. Moretti, C. Gelfi, S. Palombella, P.G. di Summa, Human platelet lysate stimulates neurotrophic properties of human adipose-derived stem cells better than Schwann cell-like cells, Stem Cell Res. Ther. 14 (1) (2023) 179.
[11] M. Cong, X. Wu, L. Zhu, G. Gu, F. Ding, G. Li, H. Shi, Anisotropic microtopography surface of chitosan scaffold regulating skin precursor-derived Schwann cells towards repair phenotype promotes neural regeneration, Regenerative Biomaterials 11 (2024).
[12] M. Saadati, O. Akhavan, H. Fazli, S. Nemati, H. Baharvand, Controlled differentiation of human neural progenitor cells on molybdenum disulfide/graphene oxide heterojunction scaffolds by photostimulation, ACS Appl. Mater. Interfaces 15 (3) (2023) 3713–3730.
[13] S. Sart, Y. Yan, Y. Li, E. Lochner, C. Zeng, T. Ma, Y. Li, Crosslinking of extracellular matrix scaffolds derived from pluripotent stem cell aggregates modulates neural differentiation, Acta Biomater. 30 (2016) 222–232.
[14] D.C. Surrao, K. Boon, B. Borys, S. Sinha, R. Kumar, J. Biernaskie, M.S. Kallos, Large-scale expansion of human skin-derived precursor cells (hSKPs) in stirred suspension bioreactors, Biotechnol. Bioeng. 113 (12) (2016) 2725–2738.
[15] J. De Kock, P. Meuleman, G. Raicevic, R.M. Rodrigues, S. Branson, K. Meganathan, V. De Boe, A. Sachinidis, G. Leroux-Roels, T. Vanhaecke, L. Lagneaux, V. Rogiers, M. Najar, Human skin-derived precursor cells are poorly immunogenic and modulate the allogeneic immune response, Stem Cell. 32 (8) (2014) 2215–2228.
[16] Y. Liu, S. Zhou, L. Zhao, X. Gu, Identification of neuronal cells in sciatic nerves of adult rats, Front. Cell. Neurosci. 16 (2022).
[17] S. Wang, H. Wang, P. Lu, L. Gong, X. Gu, M. Li, Mechanisms underlying the cell-matrixed nerve grafts repairing peripheral nerve defects, Bioact. Mater. 31 (2024) 563–577.
[18] L. Yan, S. Liu, J. Wang, X. Ding, Y. Zhao, N. Gao, Z. Xia, M. Li, Q. Wei, O.V. Okoro, Y. Sun, L. Nie, A. Shavandi, G. Jiang, J. Chen, L. Fan, Y. Weng, Constructing nerve guidance conduit using dECM-doped conductive hydrogel to promote peripheral nerve regeneration, Adv. Funct. Mater. (2024) 2402698.
[19] J.A. Biernaskie, I.A. McKenzie, J.G. Toma, F.D. Miller, Isolation of skin-derived precursors (SKPs) and differentiation and enrichment of their Schwann cell progeny, Nat. Protoc. 1 (6) (2007) 2803–2812.
[20] P. Lorenzon, K. Antos, A. Tripathi, V. Vedin, A. Berghard, P. Medini, In vivo spontaneous activity and coital-evoked inhibition of mouse accessory olfactory bulb output neurons, iScience 26 (9) (2023) 107545.
[21] T. Qi, X. Zhang, X. Gu, S. Cui, Experimental study on repairing peripheral nerve defects with novel bionic tissue engineering, Adv. Healthcare Mater. 12 (17) (2023) 2203199.
[22] S. Bolívar, E. Sanz, D. Ovelleiro, D.W. Zochodne, E. Udina, Neuron-specific RNA-sequencing reveals different responses in peripheral neurons after nerve injury, Elife 12 (2024) RP91316.
[23] Y. Gao, C. Dai, M. Zhang, J. Zhang, L. Yin, W. Li, K. Zhang, Y. Yang, Y. Zhao, Biomimetic silk fibroin hydrogel for enhanced peripheral nerve regeneration: synergistic effects of graphene oxide and fibroblast exosome, Adv. Funct. Mater. 34 (17) (2023) 2314610.
[24] R. Li, D.-h. Li, H.-y. Zhang, J. Wang, X.-k. Li, J. Xiao, Growth factors-based therapeutic strategies and their underlying signaling mechanisms for peripheral nerve regeneration, Acta Pharmacol. Sin. 41 (10) (2020) 1289–1300.
[25] L. Meng, N. Ren, M. Dong, S. Zhang, A. Wang, Z. Zhuang, J. Wang, C. Sun, H. Liu, Metal–organic frameworks for nerve repair and neural stem cell therapy, Adv. Funct. Mater. 34 (3) (2023) 2309974.
[26] M. Yu, G. Gu, M. Cong, M. Du, W. Wang, M. Shen, Q. Zhang, H. Shi, X. Gu, F. Ding, Repair of peripheral nerve defects by nerve grafts incorporated with extracellular vesicles from skin-derived precursor Schwann cells, Acta Biomater. 134 (2021) 190–203.
[27] C. Zhu, J. Huang, C. Xue, Y. Wang, S. Wang, S. Bao, R. Chen, Y. Li, Y. Gu, Skin derived precursor Schwann cell-generated acellular matrix modified chitosan/silk scaffolds for bridging rat sciatic nerve gap, Neurosci. Res. 135 (2018) 21–31.
[28] R. Kumar, S. Sinha, A. Hagner, M. Stykel, E. Raharjo, K.K. Singh, R. Midha, J. Biernaskie, Adult skin-derived precursor Schwann cells exhibit superior myelination and regeneration supportive properties compared to chronically denervated nerve-derived Schwann cells, Exp. Neurol. 278 (2016) 127–142.
[29] H.T. Khuong, R. Kumar, F. Senjaya, J. Grochmal, A. Ivanovic, A. Shakhbazau, J. Forden, A. Webb, J. Biernaskie, R. Midha, Skin derived precursor Schwann cells improve behavioral recovery for acute and delayed nerve repair, Exp. Neurol. 254 (2014) 168–179.
[30] P. Zhang, X. Lu, J. Chen, Z. Chen, Schwann cells originating from skin-derived precursors promote peripheral nerve regeneration in rats, Neural regeneration research 9 (18) (2014) 1696–1702.
[31] A. Shakhbazau, C. Mohanty, R. Kumar, R. Midha, Sensory recovery after cell therapy in peripheral nerve repair: effects of naïve and skin precursor-derived Schwann cells, J. Neurosurg. 121 (2) (2014) 423–431.
[32] L. Mu, L. Wu, S. Wu, Q. Ye, Z. Zhong, Progress in chitin/chitosan and their derivatives for biomedical applications: where we stand, Carbohydr. Polym. 343 (2024) 122233.
[33] L. Bitar, B. Isella, F. Bertella, C. Bettker Vasconcelos, J. Harings, A. Kopp, Y. van der Meer, T.J. Vaughan, L. Bortesi, Sustainable Bombyx mori's silk fibroin for biomedical applications as a molecular biotechnology challenge: a review, Int. J. Biol. Macromol. 264 (2024) 130374.
[34] M. Li, X. Cheng, S. Feng, H. Zhu, P. Lu, P. Zhang, X. Cai, P. Qiao, X. Gu, G. Wang, C. Xue, H. Wang, Skin precursor-derived Schwann cells accelerate in vivo prevascularization of tissue-engineered nerves to promote peripheral nerve regeneration, Glia 71 (7) (2023) 1755–1769.
[35] A. Urzi, I. Lahmann, L.V.N. Nguyen, B.R. Rost, A. García-Pérez, N. Lelievre, M. E. Merritt-Garza, H.C. Phan, G.J. Bassell, W. Rossoll, S. Diecke, S. Kunz, D. Schmitz, M. Gouti, Efficient generation of a self-organizing neuromuscular junction model from human pluripotent stem cells, Nat. Commun. 14 (1) (2023) 8043.
[36] D. Wu, X. Zhao, J. Xie, R. Yuan, Y. Li, Q. Yang, X. Cheng, C. Wu, J. Wu, N. Zhu, Physical modulation of mesenchymal stem cell exosomes: a new perspective for regenerative medicine, Cell Prolif. 57 (8) (2024) e13630.

[37] T. Chen, Y. Jiang, J.-P. Huang, J. Wang, Z.-K. Wang, P.-H. Ding, Essential elements for spatiotemporal delivery of growth factors within bio-scaffolds: a comprehensive strategy for enhanced tissue regeneration, J. Contr. Release 368 (2024) 97–114.
[38] E. Redolfi Riva, M. Özkan, E. Contreras, S. Pawar, C. Zinno, E. Escarda-Castro, J. Kim, P. Wieringa, F. Stellacci, S. Micera, X. Navarro, Beyond the limiting gap length: peripheral nerve regeneration through implantable nerve guidance conduits, Biomater. Sci. 12 (6) (2024) 1371–1404.
[39] Q. Wang, H. Wang, Y. Ma, X. Cao, H. Gao, Effects of electroactive materials on nerve cell behaviors and applications in peripheral nerve repair, Biomater. Sci. 10 (21) (2022) 6061–6076.
[40] X. Dong, H. Zhang, P. Duan, K. Liu, Y. Yu, W. Wei, W. Wang, Y. Liu, Q. Cheng, X. Liang, Y. Huo, L. Yan, A. Yu, H. Dai, An injectable and adaptable hydrogen sulfide delivery system for modulating neuroregenerative microenvironment, Sci. Adv. 9 (51) (2023) eadi1078.
[41] Y. Xu, X. Liu, M.A. Ahmad, Q. Ao, Y. Yu, D. Shao, T. Yu, Engineering cell-derived extracellular matrix for peripheral nerve regeneration, Mater Today Bio 27 (2024) 101125.
[42] Y. Guan, Z. Ren, B. Yang, W. Xu, W. Wu, X. Li, T. Zhang, D. Li, S. Chen, J. Bai, X. Song, Z. Jia, X. Xiong, S. He, C. Li, F. Meng, T. Wu, J. Zhang, X. Liu, H. Meng, J. Peng, Y. Wang, Dual-bionic regenerative microenvironment for peripheral nerve repair, Bioact. Mater. 26 (2023) 370–386.
[43] J.-N. Chen, X.-J. Yang, M. Cong, L.-J. Zhu, X. Wu, L.-T. Wang, L. Sha, Y. Yu, Q.-R. He, F. Ding, H. Xian, H.-Y. Shi, Promotive effect of skin precursor-derived Schwann cells on brachial plexus neurotomy and motor neuron damage repair through milieu-regulating secretome, Regenerative therapy 27 (2024) 365–380.
[44] H. Gao, Y. Liu, H. Shen, W. Guan, S. Sun, T. Zheng, L. Wu, J. Yang, G. Li, Biomimetic-inspired piezoelectric ovalbumin/BaTiO(3) scaffolds synergizing with anisotropic topology for modulating Schwann cell and DRG behavior, Int. J. Biol. Macromol. 271 (Pt 1) (2024) 132394.
[45] Y. Huo, Y. Cheng, X. Dong, Q. Cheng, X. Liang, P. Duan, Y. Yu, L. Yan, T. Qiu, Z. Pan, H. Dai, Pleiotropic effects of nitric oxide sustained-release system for peripheral nerve repair, Acta Biomater. 182 (2024) 28–41.
[46] S. Wang, C. Zhu, B. Zhang, J. Hu, J. Xu, C. Xue, S. Bao, X. Gu, F. Ding, Y. Yang, X. Gu, Y. Gu, BMSC-derived extracellular matrix better optimizes the microenvironment to support nerve regeneration, Biomaterials 280 (2022) 121251.
[47] J.G. Toma, M. Akhavan, K.J.L. Fernandes, F. Barnabé-Heider, A. Sadikot, D. R. Kaplan, F.D. Miller, Isolation of multipotent adult stem cells from the dermis of mammalian skin, Nat. Cell Biol. 3 (9) (2001) 778–784.
[48] P. Lu, G. Wang, T. Qian, X. Cai, P. Zhang, M. Li, Y. Shen, C. Xue, H. Wang, The balanced microenvironment regulated by the degradants of appropriate PLGA scaffolds and chitosan conduit promotes peripheral nerve regeneration, Materials Today Bio 12 (2021) 100158.